

P. 11/2/69



NONEQUILIBRIUM NOZZLE EXPANSIONS OF PARTIALLY DISSOCIATED AIR: A COMPARISON OF THEORY AND ELECTRON-BEAM MEASUREMENTS

W. N. MacDermott and J. C. Marshall
ARO, Inc.

July 1969

This document has been approved for public release
and sale; its distribution is unlimited.

PROPULSION WIND TUNNEL FACILITY
ARNOLD ENGINEERING DEVELOPMENT CENTER
AIR FORCE SYSTEMS COMMAND
ARNOLD AIR FORCE STATION, TENNESSEE

NOTICES

When U. S. Government drawings specifications, or other data are used for any purpose other than a definitely related Government procurement operation, the Government thereby incurs no responsibility nor any obligation whatsoever, and the fact that the Government may have formulated, furnished, or in any way supplied the said drawings, specifications, or other data, is not to be regarded by implication or otherwise, or in any manner licensing the holder or any other person or corporation, or conveying any rights or permission to manufacture, use, or sell any patented invention that may in any way be related thereto.

Qualified users may obtain copies of this report from the Defense Documentation Center.

References to named commercial products in this report are not to be considered in any sense as an endorsement of the product by the United States Air Force or the Government.

NONEQUILIBRIUM NOZZLE EXPANSIONS OF PARTIALLY
DISSOCIATED AIR: A COMPARISON OF THEORY
AND ELECTRON-BEAM MEASUREMENTS

W. N. MacDermott and J. C. Marshall
ARO, Inc.

This document has been approved for public release
and sale; its distribution is unlimited.

FOREWORD

The work reported herein was sponsored by the Arnold Engineering Development Center (AEDC), Air Force Systems Command (AFSC), under Program Element 654021F, Project 4344, Task 02.

The results of the research presented were obtained by ARO, Inc. (a subsidiary of Sverdrup & Parcel and Associates, Inc.), contract operator of AEDC, AFSC, Arnold Air Force Station, Tennessee, under Contract F40600-69-C-0001. The research was conducted from July, 1967, to June, 1968, under ARO Project No. PL3812, and the manuscript was submitted for publication on April 24, 1969.

This technical report has been reviewed and is approved.

Vincent A. Rocco
1st Lt, USAF
Research Division
Directorate of Plans
and Technology

Edward R. Feicht
Colonel, USAF
Director of Plans
and Technology

ABSTRACT

A theoretical/experimental study was made of the rapid expansion of partially dissociated air in a high enthalpy wind tunnel. The theoretical model included the important nitrogen-oxygen reaction kinetics, as well as vibrational exchanges. Pressure measurements were supplemented by electron-beam measurements of static (translational) temperature, vibrational temperature, and static density. The primary result was general confirmation of finite-rate flow calculations. Secondly, rotational temperature determination by electron beam was found to require a small empirical correction, vibrational-relaxation rates from shock experiments were inapplicable in rapid flow expansion, and the static temperature/density combination yielded the optimum comparison with theory. The nonequilibrium data were correlated with an entropy parameter for reservoir pressures from 5 to 20 atm and temperatures from 2300 to 5000° K. Verification of finite-rate theory at high density was inferred from data measured at large area ratios plus the simple nature of frozen flows downstream of the nozzle throat.

CONTENTS

	<u>Page</u>
ABSTRACT	iii
NOMENCLATURE	vii
I. INTRODUCTION	1
II. EXPERIMENTAL APPARATUS	
2.1 18-in. Low Density Wind Tunnel	3
2.2 General Instrumentation	4
2.3 Electron Beams	5
III. TEST PROCEDURE	
3.1 General	6
3.2 Reservoir Conditions	6
3.3 Sonic Flow Enthalpy Calculations	7
IV. TEST RESULTS	
4.1 Vibrational Temperature	8
4.2 Rotational Temperature	8
4.3 Density	9
4.4 Static Pressure	9
4.5 Pitot Pressure	10
V. DISCUSSION	
5.1 Theoretical Finite-Rate Nozzle Flow Calculations. . .	10
5.2 Comparison of Theory and Experiment.	16
5.3 General Correlation of Finite-Rate Effects in Nozzle Expansion	22
5.4 Results of Theoretical/Experimental Agreement . . .	24
VI. CONCLUSIONS	26
REFERENCES	28

APPENDIXES

I. ILLUSTRATIONS

Figure

1. Photograph of the 18-in. Hypersonic Wind Tunnel	35
2. Sketch of the 18-in. Hypersonic Wind Tunnel	36
3. Arrangement of Components in the Test Chamber	37
4. Electron-Beam Installation	
a. Electron-Beam Installation for Temperature Measurement	38
b. Photograph of Flow with Electron Beam Used for Temperature Measurement	39

<u>Figure</u>	<u>Page</u>
5. Electron-Beam Installation for Density Measurement	40
6. Reservoir Conditions for Individual Runs.	41
7. Comparison of Total Enthalpy from Energy Balance and Sonic Flow Calculation.	42
8. Effect of Throat Contamination on Indicated Sonic Flow Enthalpy, Assumed $d^* = 0.200 \pm 0.004$ in.	43
9. Impact Pressure Profiles across the Flow at the Nozzle Exit.	44
10. Static Temperature versus Area Ratio for Various Types of Expansion, $p_{t1} = 10$ atm, $T_{t1} = 4000^\circ\text{K}$	45
11. Finite-Rate Flow Regions and Velocity in Nozzle, $p_{t1} = 10$ atm, $T_{t1} = 4000^\circ\text{K}$	46
12. Nitrogen Vibrational Relaxation Time Factor versus Temperature	47
13. Experimental and Theoretical Static Temperature versus Area Ratio	
a. $p_{t1} = 20$ atm, $T_{t1} = 2300^\circ\text{K}$	48
b. $p_{t1} = 10$ atm, $T_{t1} = 4000^\circ\text{K}$	49
c. $p_{t1} = 5$ atm, $T_{t1} = 5000^\circ\text{K}$	50
14. Experimental and Theoretical Static Temperature versus Static Density	
a. $p_{t1} = 20$ atm, $T_{t1} = 2300^\circ\text{K}$	51
b. $p_{t1} = 10$ atm, $T_{t1} = 4000^\circ\text{K}$	52
c. $p_{t1} = 5$ atm, $T_{t1} = 5000^\circ\text{K}$	53
15. Average Deviation of Measured Static Temperature from Finite-Rate Theory for Ten Reservoir Conditions, $p_{t1} = 5$ to 20 atm, $T_{t1} = 2300$ to 5000°K	54
16. General Correlation of Finite-Rate Effect on Static Temperature and Static Pressure	
a. T_1/T_{1EQ} versus Σ	55
b. p_1/p_{1EQ} versus Σ	56

	<u>Page</u>
II. TABLES	
I. Summary of Reservoir Conditions and Measurements at Nozzle Exit	57
II. Reactions Included in Finite-Rate Flow Model	58
III. TEMPERATURE MEASUREMENTS BY THE ELECTRON-BEAM TECHNIQUE	59
IV. DETERMINATION OF DENSITY BY ELECTRON BEAM	64

NOMENCLATURE

A	Atomic weight of a nucleus
A/A*	Effective area ratio of flow
C _p	Parameter in pressure distribution relation, Eq. (1)
D _{i,j}	Logarithmic derivative of v _i with respect to v _j
d*	Diameter of nozzle throat
Ev _g	Vibrational energy of molecule in v _g vibrational state
e	Electric charge on electron
H	Enthalpy
I	Intensity of emission
i	Electron-beam current
K	Rotational state quantum number
k	Boltzmann constant
M	Mach number
N _a	Avogadro's number
N ₀	Number density of neutral N ₂ molecules
n	Number density of atomic nuclei
P	Relative vibrational transition probability
p	Pressure

Q_v	Vibrational state sum
R	Gas constant for low temperature air
$R_{i,j}$	Ratio of experimental to theoretical value of variables
r^*	Radius of throat of nozzle
r_e	Classical radius of electron
S	Entropy
T	Temperature
V	Velocity
v	Vibrational state quantum number
v_i	Value of a specific thermodynamic variable
x	Length coordinate along nozzle or along electron beam
Z	Compressibility factor or atomic number of nucleus
β	Ratio, electron speed/speed of light
γ	Specific heat ratio
δ	Angle of deflection of electron
ϵ	Percent error in a variable
θ	Nozzle half-angle
θ_{rot}	Characteristic rotational temperature of N_2 molecule in ground vibrational state, 2.89°K
λ	Rate of deflection of electron through a given angle per unit solid angle per unit length of beam
$\bar{\nu}$	Wave number of energy transition
ρ	Mass density
Σ	Reservoir entropy parameter, defined by Eq. (8)
σ	Scattering cross section of a nucleus
τ	Vibrational relaxation time
τ_c	Characteristic expansion rate parameter
Ω	Solid angle into which electrons are deflected

SUBSCRIPTS

1	Condition upstream of normal shock wave
2	Condition downstream of normal shock wave
EB	Value determined by energy balance
EQ	Value in equilibrium flow
eff	Effective
exp	Experimental value
fr	Value in frozen flow
g	Ground state of neutral N ₂
i, j	Indices specifying specific variables, Eq. (3)
R	Rotational
sonic	Value determined by sonic flow calculation
t	Total or stagnation value
theor	Theoretical value
v	Vibrational
∞	Condition in free stream

SUPERSCRIPTS

'	Excited electronic energy state of N ₂ ⁺ ion
''	Ground electronic energy state of N ₂ ⁺ ion

SECTION I INTRODUCTION

In the past decade, large strides have been made in the theory of gas dynamic flow expansions in which changing composition caused by high-speed chemical reactions is a distinctive part of the flow. Impetus for these developments has come from the design requirements of high performance rocket nozzles and high enthalpy wind tunnel nozzles. The first problem encountered was the evaluation of the basic thermodynamic properties of high temperature gas in equilibrium. These properties have now been worked out in great detail for high enthalpy air (Ref. 1), and they form the fundamental basis for all nozzle performance calculations for advanced wind tunnels. The second major problem encountered was that of formulating a theory of flow expansion which accounted for the characteristic finite rate of various chemical reactions in relation to the rate of thermodynamic expansion in nozzle flows. Beginning with a model of a simple binary gas subject to sudden freezing of chemical reactions, the finite-rate expansion theories have evolved to the current theories which allow for an arbitrary number of gas constituents, an arbitrary number of interacting chemical reactions and vibrational energy exchanges, and gradual departures from equilibrium and approach to frozen flow (Refs. 2 through 6).

Nozzle flows producing vibrational, chemical, and ionic nonequilibrium have been studied, but generally, the flow regimes have been such that the translational and rotational degrees of freedom have been assumed to remain equilibrated. It is generally accepted that the latest theoretical formulations reproduce in every important respect the actual physical and chemical phenomena prevailing in nonequilibrium nozzle flows.

Experimental verification has lagged behind the development of this nonequilibrium theory, mainly because of the increased demands placed on instrumentation technology. It is necessary to distinguish between verification of a flow theory and flow calibrations made subsequent to that verification. For example, the thermodynamic model of flow in a low temperature wind tunnel nozzle is an isentropic expansion with a constant specific heat ratio. Verification that this model correctly represents the flow process requires, in addition to measurement of the state in the nozzle reservoir, measurement of two independent variables at some point in the flowing gas. Once the adequacy of the flow model is established, however, further routine flow determinations require only a single measurement in the flowing gas, and this is found to be generally true regardless of the complexity of the flow model. The

validation of the flow model, on the other hand, definitely increases in complexity as the flow model increases in complexity. In principle, one more independent measurement in the flow is required for each additional degree of freedom which is activated at high temperature in the reservoir and can potentially depart from equilibrium in the expansion. Because the number of independent measurements that can be made in a flowing gas is limited, exact verification of a finite-rate expansion theory is feasible only for the simplest gases. The degrees of freedom activated in high temperature air far outnumber the available measurements, so that verification of a flow model in the exact sense is currently unattainable. This is not to say that partial verification is not possible or desirable. Confidence in a nonequilibrium air model can be maximized, if not made absolute, by simply making as many flow measurements as possible, particularly if some of these measurements are especially sensitive to nonequilibrium effects.

The first attempts to check nonequilibrium theories in air were limited to the conventional pressure measurements in the flow, static and pitot pressures. Pitot pressure is relatively insensitive, but static pressure is moderately sensitive to nonequilibrium effects, so that at least an initial confidence level was established when these measurements exhibited reasonable agreement with contemporary theories (Refs. 7 and 8). In recent years, a new group of diagnostic measurements has become available with the development of the electron-beam probe. In its various forms, this technique has added static temperature, static density, and vibrational temperature to the list of parameters which can be measured in a flowing gas. Although it has been most extensively applied in unheated low density free jets and nozzle expansions, it has recently been applied to a number of high enthalpy nozzle expansions in which departures from equilibrium occur (Refs. 9 and 10). It represents an especially valuable technique for such studies because the static (translational and rotational) temperature is the most sensitive thermodynamic parameter to nonequilibrium effects in a flowing gas. These increased measuring capabilities have already indicated needed corrections to finite-rate theories by confirming and strengthening earlier evidence (Ref. 11) that vibrational relaxation rates obtained in shock experiments are not valid for rapidly expanding flows (Refs. 10, 12, and 13). This fact has even more recently been substantiated by an infrared band-reversal technique (Ref. 14).

A general outline of the electron-beam technique of temperature measurements as originally formulated by Muntz (Ref. 15) and later modified by others (Refs. 16 and 17) is given in Appendix III. Several different techniques have been used to measure density by an electron

beam (Refs. 10, 15, and 18), but the scattering technique reported in Refs. 12 and 19 was used in the current investigation and is briefly described in Appendix IV. The electron beam is a very powerful diagnostic technique, but it is inherently limited to very low gas pressures, normally 1 torr and below. Consequently, the finite-rate expansions of practical interest can be studied by this technique only after the expansion has proceeded to very large area ratios and high hypersonic Mach numbers, far beyond the point in the flow where the departures from equilibrium occur. It will be seen later that, in many respects, this is not really a very serious limitation. There is also a limitation expressed by the current uncertainty over the accuracy of the excitation-emission model of Ref. 15. The results of some experiments have seemed to indicate that, for purposes of temperature determination at least, an empirical correction to this model must be made (Refs. 16 and 20). The rather considerable effort in this field in the past few years is summarized in Appendix III. Fortunately, in the static temperature range used in the present study, this uncertainty is only 10 percent or less.

In the present work, an effort was made to extend the experimental verification of a finite-rate-expansion theory to a sufficient range in reservoir conditions that the correlation of the nonequilibrium effects with reservoir entropy could be explored, as done in Refs. 21 and 22, for purely theoretical solutions. The usual pressure measurements in the flow were supplemented by the electron-beam measurements referred to above, and major attention was focused on the stream static temperature, since it displayed the greatest sensitivity to nonequilibrium. The pressure and temperature regime available in the experimental facility to be used was such that it was necessary to develop a machine calculation program for a finite-rate expansion allowing for departures from equilibrium upstream of a nozzle throat and in which the chemical and vibrational reactions simultaneously proceeded at finite rates. To this end, the air model was slightly simplified by neglecting the minor constituents, argon (Ar), carbon dioxide (CO₂), and all ionic species.

SECTION II

EXPERIMENTAL APPARATUS

2.1 18-IN. LOW DENSITY WIND TUNNEL

The nonequilibrium expansions studied in the investigation were produced in a low density hypervelocity wind tunnel supplied with air

heated to high enthalpy in a 250-kw, d-c arc heater (Figs. 1, 2, and 3, Appendix I). A small stilling chamber is used downstream of the heater, followed by a simple conical nozzle which expands the flow into an open-jet test section. The test section is continuously pumped by a six-stage steam ejector. The reservoir conditions produced for this test were total pressures from 5 to 20 atm, total enthalpies from 1150 to 4160 Btu/lb_m, and stagnation temperatures from 2300 to 5000°K.

The expansion nozzle used had a throat diameter of 0.200 in., an exit diameter of 18 in., a conical half-angle of 10 deg, and a geometric area ratio of 8100. With the above reservoir conditions, the static pressure at the nozzle exit was in the range from 10×10^{-3} to 31×10^{-3} torr, and the static temperature at the nozzle exit was from 50 to 140°K. This rarefied flow, at mass flows from 0.01 to 0.05 lb_m/sec, was pumped through the test section with all six stages of the steam ejector operating.

2.2 GENERAL INSTRUMENTATION

The general location of diagnostic measurements was selected as the exit plane of the nozzle. Pitot pressures were measured 1 in. from the nozzle centerline in a plane 1 in. downstream of the nozzle exit. The pitot-pressure measurement used directly for diagnostic purposes was made with an uncooled, flat-faced tube having an outside diameter of 0.25 in. Pitot-pressure profiles were obtained with a flat-faced, water-cooled probe, 0.5 in. in diameter. Comparison of pressures measured by these two probes indicated that low density effects on pitot pressure were negligible for this test. Measured pitot pressures ranged from 3 to 8 torr.

The static pressure was measured on the nozzle wall, 1 in. upstream of the nozzle exit. The orifice diameter was 0.25 in. Conditions at this orifice were such as to require a low density correction of the type discussed in Refs. 23 through 25. Capacitance-type transducers were used to measure both the pitot and static pressures.

Nozzle reservoir conditions were primarily determined by the energy-balance technique, although a few checks of enthalpy by the sonic flow method were made. The energy balance requires precise measurements of heater input power, air mass flow, and energy removed by cooling up to the throat. Input power is determined by precise voltage and current measurements at the heater electrodes. Cooling power is determined by water volume flow measurement with

a calibrated turbine-type flowmeter and by the temperature rise measured by a ten-element thermopile. The air mass flow is measured by a sharp-edged orifice with the pressure differential sensed by a strain-gage-type pressure transducer. Inlet temperature at the orifice is measured by a copper-constantan thermocouple.

2.3 ELECTRON BEAMS

The electron beams were projected across the nozzle exit flow, 1 in. downstream of the nozzle exit and intersecting the longitudinal axis of the nozzle. Because of conflicting requirements of the temperature and density measurements, two separate electron-gun installations were used. It was not possible to test with both electron beams mounted in the test cell simultaneously. Separate tunnel entries were used for the temperature and density measurements and the two sets of data were related by using the pitot pressure as a transfer parameter for a given reservoir condition.

2.3.1 Temperature Measurement

The temperature measurements were made with a converted electron-beam welding gun which produced a 2-ma, 20,000-v beam. This gun was mounted inside the test section above the free jet and gave a vertical beam (Fig. 4). The optical detection system consisted of a 21-in. focal length collimating lens inside the test section, a similar condensing lens outside the test section, and 0.75-meter diffraction grating spectrometer located outside the test section. This system was focused on a small segment of the vertical electron beam at the nozzle centerline. The radiation detector used on the spectrometer was a Hamamatsu R106 multiplier phototube having an S-19 spectral response.

2.3.2 Density Measurement

Density measurements were made with a television tube electron-gun element which produced a 50-ma beam at 40,000 v. This beam was injected horizontally across the nozzle flow (Fig. 5). The detector for the scattered electrons of the density measurement was located inside the test section, shielded by a collimator, and placed above the horizontal beam in such a position that electrons scattered out of the beam at an angle of 45 deg from the beam were detected. The detector element itself was a silicon surface-barrier detector.

SECTION III TEST PROCEDURE

3.1 GENERAL

As in most arc heater facilities, it is very difficult to obtain precise repetition of reservoir conditions from run to run in the 18-in. low density wind tunnel. Rather than attempting to attain such repetition, the reservoir pressure was held as closely as possible to a desired value, and the stagnation enthalpy was allowed to seek its own level, determined by the heater efficiency and power settings for each run. The result was a series of runs at essentially constant p_{t1} (5, 10, 15, and 20 atm) and with H_{t1} ranging over rather wide limits. The basic flow diagnostic data measured at the nozzle exit were then plotted as functions of H_{t1} at constant p_{t1} . These experimental plots of p_1 , p_{t2} , T_1 , T_v , and ρ_1 were faired, and the faired curves were used to extract values of these parameters at even values of $T_{t1} = 2300, 3000, 4000$, and 5000°K . These are the values tabulated in Table I (Appendix II). It has already been noted that the temperature and density data were measured on different tunnel entries and that pitot pressure was used as a transfer parameter for these two sets of data.

3.2 RESERVOIR CONDITIONS

The reservoir enthalpy (H_{t1}) was routinely determined by the energy-balance method. The accuracy of this determination was evaluated two ways: First, a theoretical error analysis of all the individual measurements entering into the energy-balance calculation indicated an overall accuracy of ± 3 percent or a total uncertainty interval of 6 percent for $(H_{t1})_{EB}$. Second, a number of check calculations of enthalpy by the sonic flow method were made, as discussed in the next section.

A summary plot of individual reservoir conditions obtained during this investigation is given in Fig. 6. Curves of constant compressibility factor (Z) are superimposed on these data to indicate the degree of dissociation varied from essentially 0 percent below 2500°K to a maximum of 20 percent at 5300°K . The reservoir conditions for the points referred to in Section 3.1 are given in Table I, in terms of p_{t1} , T_{t1} , H_{t1} , ρ_1 , Z , and the specific heat ratio corresponding to frozen conditions at the reservoir composition ($\gamma_{fr,t}$).

3.3 SONIC FLOW ENTHALPY CALCULATIONS

Among the factors entering into the enthalpy calculation by the sonic flow method, the throat area was considered to possess the greatest uncertainty, especially during the latter stages of a long run when there was an unknown amount of deposition on the throat. This deposition is the result of progressive heater electrode erosion during operation, which leaves a fine deposit on the throat section. A routine cleaning operation by brushing and air blasting is sufficient to remove most of this deposit between runs. However, there is often a very thin persistent layer remaining which can only be removed by ultrasonic cleaning. After such a cleaning, the throat dimension is precisely 0.207 in., as determined by an optical comparator. Removal of the nozzle throat from the tunnel for either ultrasonic cleaning or optical measurement of d^* is not convenient during extended tunnel operation, and it is simply assumed that after the routine cleaning operation the throat diameter is 0.200 ± 0.004 in.

In Fig. 7 is given a comparison of $(H_{t1})_{EB}$ with $(H_{t1})_{sonic}$ for the initial point of 16 runs, where d^* was assumed equal to 0.200 ± 0.004 in., or, in four cases, equal to a precise optically measured value before the run. The tolerance shown on most of the sonic flow values corresponds to the tolerance in d^* . There is an evident statistical scatter of these values about the calculated ± 3 -percent scatter band of the $(H_{t1})_{EB}$ values. Note that three of the four points for which d^* was precisely measured fall within this ± 3 -percent band.

For any points other than the initial points in a run, the throat dimension was even more uncertain than 0.200 ± 0.004 in. The steady, but unknown, deposition of eroded electrode material on the throat produced a systematic divergence of the two enthalpy calculations for successive points in a run, when a constant throat area was used in the sonic flow calculation (Fig. 8). Of course, there were differences in time between points from run to run, and probably differences in deposition rate also, but an obvious upward trend in $(H_{t1})_{sonic}$ is shown in this figure, which represents an average of a number of runs. The convergence of $(H_{t1})_{EB}$ and $(H_{t1})_{sonic}$ for the initial points in the runs, however, is supporting evidence for the acceptance of the energy-balance calculation for all points of a run, since the throat area does not enter into this calculation.

SECTION IV TEST RESULTS

In addition to the reservoir data, Table I also gives tabulated values of the test section diagnostic measurements of vibrational temperature, rotational temperature, density, static pressure, and pitot pressure. The pressure and density data are nondimensionalized by reservoir values, and effective area ratios for these data are given as obtained from finite-rate expansion calculations described in Section V. These data are definitely experimental data, but they have been interpolated to even values of T_{t1} . Each of the test section measurements must be examined in the light of certain qualifications described below.

4.1 VIBRATIONAL TEMPERATURE

The vibrational temperatures were determined from nitrogen (N_2) molecular band intensity ratios in the electron-beam emission (Refs. 10 and 15 and Appendix III). The measured temperatures were found to be uniformly lower than values predicted by finite-rate expansion calculations using vibrational relaxation rates obtained in shock tube studies. The differences can be seen in Table I as ranging from 195 to 1334°K, depending on the reservoir condition. This same result has been found in other facilities by different techniques, and it is now generally accepted that vibrational relaxation times obtained in shock experiments are not directly applicable in rapid expansions. The magnifications required on the relaxation rates to bring the calculated values of vibrational temperature into agreement with the presently measured values range from 4.4 to 28 and are tabulated in Table I. It was found that increasing the vibrational rates by these amounts had a very small effect on the static (translational) temperatures in the finite-rate expansions.

4.2 ROTATIONAL TEMPERATURE

The rotational temperatures were determined by the distribution of rotational line intensities within a certain molecular band radiation observed in the electron beam (Refs. 9, 15, and 16 and Appendix III). Again, the radiation used is from N_2 species so that, strictly speaking, the measured values are N_2 molecule rotational temperatures in the flow. Calculations have been made, however, which support the assumption of rotational equilibrium. Thus, it is a good assumption that the N_2 molecule rotational temperature is equal to the translational temperature of all species.

Because of an uncertainty as to the basic theory of the rotational temperature measuring technique (Appendix III), the direct experimental values of T_R are supplemented in Table I by values which have been empirically corrected by the Robben-Talbot factor (Ref. 16). It will be seen in Section V that the corrected values appear to be more consistent with the finite-rate calculations.

4.3 DENSITY

The static density in the flow was determined in a straightforward way by counting electrons scattered out of a sensitive volume in a given direction (Appendix IV). This technique allows an extremely simple and straightforward static calibration technique. The scatter in the static calibration curves was found to be approximately 10 percent, so that the density measurement must be considered to possess at least this degree of inaccuracy.

4.4 STATIC PRESSURE

The static pressure was subject to two appreciable corrections, a geometric correction and a low density correction. The geometric correction was necessitated by the gradients in the flow between the static pressure orifice on the nozzle wall and the main diagnostic point on the nozzle centerline. The gradients transverse to the flow were fairly large, as can be seen in the pitot-pressure profiles of Fig. 9, but the gradients in the streamwise direction were found to be small. The procedure for inferring the geometric correction to the static pressure involved (1) transfer of static pressure from the wall orifice to the edge of the boundary layer by the standard assumption of negligible transverse pressure gradient in the boundary layer and (2) relating of static pressure at the edge of the boundary layer to the static pressure at the nozzle centerline by use of the pitot-pressure profiles and an assumed isentropy in the frozen flow in the test core.

The low density correction to static pressure was of the type described in Refs. 23 through 25. This low density orifice effect is opposite in sense to the geometric correction; that is, it increases the inferred true static pressure over that sensed by the orifice. At the highest T_{t1} and lowest p_{t1} , the low density correction predominates, and the net correction to the measured static pressure is a 22-percent increase. At the lowest T_{t1} and highest p_{t1} , the geometric correction predominates, and the net correction to the measured static pressure is a reduction of 30 percent (Table I).

4.5 PITOT PRESSURE

The low density effect on pitot pressure was calculated to be no more than from 2 to 3 percent for the range of conditions covered in the present test. This result was confirmed by the agreement of p_{t2} data taken with the 0.25-in. probe and the 0.50-in. probe. Therefore, no low density corrections were made to the pitot pressure in the process of analyzing the diagnostic data. Finite-rate calculation of the flow behind the probe shock wave was beyond the scope of the present study, and pitot pressure was simply assumed to be equal to $0.92 \rho_1 V_1^2$, a good approximation for hypersonic frozen flow.

SECTION V DISCUSSION

The fundamental purpose of this entire investigation was twofold: to study the adequacy of the electron-beam techniques as diagnostic tools and to investigate the accuracy of finite-rate expansion calculations for nonequilibrium flows in high enthalpy nozzles, specifically the nozzle of the 18-in. low density wind tunnel.

5.1 THEORETICAL FINITE-RATE NOZZLE FLOW CALCULATIONS

The development of theoretical models for calculation of flow behavior in nonequilibrium nozzle expansions has progressed to the point where nearly every potential finite-rate effect is allowed for (Ref. 26). For use in the present study, a calculational procedure was developed which is similar in principle to that of Ref. 17 but which is slightly simplified in several respects to facilitate ready availability of solutions. A modified air model was assumed in which the trace species Ar, CO₂, neon (Ne), and ionized species were neglected. Nevertheless, all the important features of the energetically important N₂ and oxygen (O₂) dissociation/recombination reactions and the nitric oxide (NO) "shuffle reactions" were included, as shown in Table II. Ionization was neglected because the anticipated stagnation temperatures were less than 6000°K. The only chemical species included were N₂, N, O₂, O, and NO. In the final programmed calculation, the relative amounts of N₂ and O₂ in the low temperature composition can be varied as desired, including the extremes of pure N₂ or O₂. For the calculations presented herein, the composition was taken to consist of 0.79124 moles of N₂ and 0.20876 moles of O₂, per mole of air. The flow is assumed to be one-dimensional, and the calculation is carried out by the method of

Ref. 27, using the mass, momentum, and energy conservation equations, the gas equation of state, the caloric equation of state, the chemical specie production equations, and the vibrational energy exchange equations, all in differential form. Internal energy of the gas is determined from the partition functions for each chemical specie, summed over all species present. The partition functions include terms for translational, rotational, vibrational, and electronic energy, and a heat of formation term to account for the energy required to produce each specie from the standard state of the gas at low temperature. The standard state consists only of N_2 and O_2 molecules. When the flow is essentially in thermodynamic equilibrium, as it is assumed to be in the reservoir, the chemical composition is determined from the basic dissociation equations for the three molecular species. The equilibrium constants for these reactions are determined from the partition functions of the reacting species. In the nonequilibrium part of the expansion, the total production rate of each specie is calculated from the dissociation reactions and the NO shuffle reactions. These shuffle reactions are somewhat faster than the dissociation reactions, since they require no third-body catalytic agent, and thus tend to keep the composition closer to equilibrium. The reverse (recombination) rates for the reactions included are given in Table II. The dissociation rates are determined from the recombination rates and the equilibrium constants.

The usual procedure in performing calculations of this type is to specify the nozzle area ratio as some analytic function of the axial dimension (x) and to relate this to the thermodynamic solution by evaluating the differential equations as functions of the x -coordinate also. This works satisfactorily when the flow conditions are such as to delay the departures from equilibrium until the flow is in the supersonic part of the nozzle. However, when nonequilibrium effects must be included in the subsonic flow and through the throat region, the double-valued nature of the area-ratio function makes the solution very difficult by this method. In the present case, the method of Ref. 27 was used, in which the static temperature was taken as the independent variable, and the flow was related to the nozzle geometry by specifying the static pressure as a function of the x -coordinate. Although any analytic function that is monotonically decreasing will do, a study of several existing nozzle flow solutions indicated that the simple function

$$p = p_{t_1} e^{-C_p x^2} \quad (1)$$

would closely fit the calculated pressure distributions. Downstream of the nozzle throat (arbitrarily at $M = 1.10$), the area ratio function is specified. Currently, two successive cubic equations are used. The

constants in the first equation are selected so that the flow properties and their derivatives are continuous at the match point between the pressure function and the area-ratio function. The use of static temperature as the independent variable is a natural choice since the partition functions, their derivatives, the chemical production-rate parameters, and the vibrational relaxation-rate parameters are all functions primarily of temperature.

Particular care must be exercised at the beginning of the nonequilibrium solution. If the flow is very nearly an equilibrium flow, arithmetic inaccuracies may result from the requirement of finding small differences between two large numbers. This problem is discussed in detail in Ref. 5. In addition, very small step sizes are required to maintain computational stability even when sufficient numerical accuracy is available. The result is long computational times. Experience has shown that an equilibrium solution may be carried out for some distance down the nozzle until the chemical production rates indicate a significant lag in the atomic recombination as compared to that required to maintain an equilibrium composition. Typically, the equilibrium calculation can be retained until the actual recombination rates are approximately 5 percent less than those required by the equilibrium expansion (Ref. 28). The method used for selecting the starting point of the nonequilibrium solution is essentially that of this reference, although the initial conditions are taken to be those from the equilibrium solution, as proposed by Emanuel and Vincenti (Ref. 5).

The initial step size for the nonequilibrium solution is calculated to correspond to the smallest characteristic length of the chemical reaction system (Appendix III of Ref. 5). Thereafter in the solution, the maximum allowable step size is related to the shortest characteristic length among those from both the chemical and vibrational reactions. The relationship between characteristic length and maximum step size to retain arithmetic stability depends on the method of extrapolation used. According to Ref. 5, a fourth-order Runge-Kutta method is stable for step sizes up to 5.7 times the minimum characteristic length. For a first-order (or linear) extrapolation method, the allowable ratio is ≤ 2.0 .

The method of extrapolating the differential equations now in use is a compromise between the simplest assumption of constant gradients over a small increment and the complex calculations of the Runge-Kutta method. The gradient of each dependent variable is assumed to vary linearly with temperature about the latest point in the calculations. The rate of variation is determined by comparing the last two calculated values of the gradient. A mean value of the gradient over the succeeding

step is then estimated, and this mean value is used to calculate the next value of the variable. The dependent variables thus extrapolated include the static pressure, the vibrational temperatures, and the chemical specie concentrations. The density, enthalpy, and velocity are then calculated, and a new set of gradients is evaluated. For each of the extrapolations, the estimated mean value of the gradient is compared with the last calculated value. Significant variations indicate either a large step size or large second derivatives of the variables, suggesting that the linear approximation may not be accurate over that large an increment of the flow. If the gradient varies across an increment by more than a specified upper limit, the step size is reduced by a specified factor, typically 1.4. If all gradient variations are below the upper limit for ten consecutive steps, they are compared to a lower limit, which is related to the upper limit as suggested in Ref. 5. When all gradient variations are below the lower limit, the step size is increased by the same specified factor. By this technique and the imposition of the stability limits on step size, the calculation is allowed to progress as rapidly as possible while maintaining arithmetic accuracy.

The computational procedure described above has been programmed in FORTRAN IV (E) language for calculation on an IBM 360/50 computer. Flow solutions have been obtained over the range of reservoir conditions pertinent to the experimental study reported herein for the nozzle geometry of the 18-in. low density wind tunnel, described in Section 2.1. In these cases, the nonequilibrium solutions were started at temperatures within 5 to 65°K of the stilling chamber temperature, corresponding to Mach numbers between 0.13 and 0.43. Chemical "freezing" occurs very rapidly, being essentially complete at the sonic point. Vibrational energy relaxation continues further downstream, depending on the values of the rate parameter used. For these solutions, the average computer run time was approximately 2.5 min. For nozzles of a significantly larger scale or for much higher reservoir pressures, the flow would remain near equilibrium much further downstream. In these cases, the computer time would be somewhat longer, although not unreasonably long.

Two additional features have been developed and written in the FORTRAN IV (E) computer language, although they have not as yet been utilized in actual calculations. One of these features a set of coupling factors which attempts to assess the interaction of vibrational nonequilibrium on chemical reaction rates and chemical nonequilibrium on vibrational relaxation rates. The form of the coupling factors was taken from Ref. 29. The second new feature consists of the modified fourth-order Runge-Kutta extrapolation technique as described in Refs. 26, 30, and 31. If use of the coupling factors or changes in the flow properties

and nozzle geometry result in unacceptably long computer run times, the use of this more advanced procedure may result in significant gains. Several researchers have reported drastic reductions in computational time as a result of the increased accuracy which this technique provides, thus permitting larger step sizes.

5.1.1 Results of Finite-Rate Calculations

The net effect of nonequilibrium on a nozzle flow may be considered as the combined effect of changes in final chemical composition and consequent changes in the final values of the thermodynamic variables. Measurement of chemical composition of a flowing gas is very difficult. Mass spectrometric techniques are under development (Ref. 32) but are not yet considered sufficiently developed to provide a comprehensive analysis of nonequilibrium flows. Thus, attention is directed to the thermodynamic variables which can be measured with reasonable accuracy. The typical freezing of chemical reactions and vibrational energy exchanges in a finite-rate nozzle expansion leaves the flow in such a condition that atomic species and vibrationally excited molecules are unnaturally present at low temperatures. The energy of recombination, which would have been released to the flow had those atoms recombined, and the vibrational energy, which would have been released had the vibrational degrees of freedom remained equilibrated, represent a withholding of a certain amount of thermal energy from the flow, in other words, an "effective" heat removal from the flow. This heat removal is the primary effect of nonequilibrium on the flow. It leads to a decrease of temperature, pressure, and velocity and an increase in density. A secondary effect of nonequilibrium is the imposition of non-unity values of the gas compressibility factor (Z) at low temperatures. This produces small changes in the interrelationships of p , ρ , and T , but the general effect of heat removal is dominant. It is invariably found that the largest effect of nonequilibrium involves temperature, followed by pressure and density, in that order.

It is possible to express the cumulative nonequilibrium effects in terms of changes in the related values of any two of the thermodynamic parameters. Since each of these variables undergoes changes of varying degree, however, it is often more revealing to isolate the effect on a single thermodynamic variable by expressing it as a function of area ratio as the independent variable. Figure 10 gives the variation of static temperature with area ratio for expansions from $p_{t1} = 10$ atm and $T_{t1} = 4000^\circ\text{K}$, comparing the finite-rate solution with various limiting cases. In fundamental terms, the effect of the kinetic model is simply to change the rate at which the static temperature decreases in

the expansion. This temperature decrease is the result of conversion of disordered energy (chemical and thermal) to directed kinetic energy of flow. The number of activated degrees of freedom which participate in this conversion determines the rate at which the temperature of any one of them decreases. Thus, there are the following cases in order of rate of decrease of temperature:

1. Complete Equilibrium. All of the activated high temperature degrees of freedom participate in the energy conversion, giving the slowest temperature decrease with area ratio and an effective specific heat ratio of 1.269.
2. Finite Rate. All of the activated high temperature degrees of freedom participate for only a short initial segment of the flow, after which they, one by one, become incapable of keeping pace with the rapidly changing thermodynamic parameters. The result is a greater rate of decrease in temperature.
3. Completely Frozen Expansion. The high temperature degrees of freedom are considered to be so sluggish that they do not contribute to energy conversion at all. They remain activated at the reservoir temperature level, and the kinetic energy of flow comes only from the translational and rotational energy of the molecules. The rate of decrease of temperature is further increased. The expansion is isentropic with a constant $\gamma = 1.44$, determined by the frozen composition in the reservoir of 85-percent molecules and 15-percent atoms for the pressure and temperature of Fig. 10.
4. Monatomic Gas. This case is not related to the present air model but is presented simply to show the ultimate limiting case of expansion with the minimum possible number of degrees of freedom (three) feeding the energy conversion. This, of course, gives the maximum rate of decrease of temperature, corresponding to $\gamma = 1.667$.

It is noted that the nonequilibrium effect on static temperature is quite small in the subsonic part of the expansion, but it grows rapidly in the supersonic portions. The finite-rate effect has decreased the temperature at the throat only 5 percent below the equilibrium value, whereas at $A/A^* = 2.0$ the decrease is 26 percent, and this grows to a 70-percent reduction at $A/A^* = 1000$. At $A/A^* > 100$, the nonequilibrium effect on static temperature is nearly constant. It would be very difficult to experimentally ascertain finite-rate effects in subsonic (or even sonic) flow. Obviously, there is a fundamental advantage to be gained by studying nonequilibrium effects at large area ratios, and this is consistent with the basic low density limitation of the electron-beam technique.

The nonequilibrium effect on vibrational temperature is much larger than on static temperature. The variation of the N_2 molecule vibrational temperature is also shown in Fig. 10, and it is seen that this temperature freezes out at a very high level, 3433°K, whereas the static temperature drops to very low values. This curve results from the finite-rate calculation using vibrational-rate data for N_2 obtained in shock experiments.

It is interesting to observe the actual physical extent of the regions in the flow in which the finite-rate effects occur. These regions are displayed in Fig. 11 for the reservoir condition of Fig. 10, together with part of a full-scale nozzle contour. Nonequilibrium regions for four chemical species and three vibrating molecules are given. These regions are arbitrarily defined by a 1-percent deviation from equilibrium and an approach to within 1 percent of final frozen values. All departures from equilibrium occur upstream of the throat. It is particularly interesting that the chemical finite-rate region for N_2 lies entirely upstream of the throat. Atomic N is not a significant component anywhere in this expansion. The total extent of nozzle flow in which finite-rate conditions exist is only 1.9 in. out of a total nozzle length of 51 in. Further, if only the energetically important reactions are considered (O_2 dissociation, N_2 vibration), the finite-rate region covers only 0.75 in. around the nozzle throat. The important finite-rate effects are completed by a supersonic area ratio of 2.2, and the finite-rate temperature versus area-ratio curve of Fig. 10 represents a constant- γ frozen flow beyond this point. Flow velocity for equilibrium and finite-rate expansion is also given in Fig. 11.

5.2 COMPARISON OF THEORY AND EXPERIMENT.

The two experimental points in Fig. 10 for vibrational and static temperature at $p_{t1} = 10$ atm and $T_{t1} = 4000^\circ K$ show the general result found at all reservoir conditions, that the initial vibrational temperature calculations were much farther from the measured data than were the static temperatures.

5.2.1 Vibrational Temperature and Vibrational Relaxation Rate

The N_2 molecule vibrational temperatures were determined by analysis of the relative intensities of the (0, 1) and (1, 2) vibrational bands of the N_2^+ first negative system excited by the electron beam (Appendix III). The vibrational-rate characteristic of the N_2 molecule which was initially used in the finite-rate calculation was the relation

$$\tau_p = 6.338 \times 10^{-13} \left[1 - \exp \left(- \frac{3337}{T_1} \right) \right] T_1^{1/2} \exp \left(\frac{192}{T_1^{1/4}} \right) \text{ atm-sec} \quad (2)$$

where T_1 is in degrees Kelvin. This is an empirical relation, with form based on transition probability theory, representing a large amount of relaxation data obtained in shock wave experiments, e. g., those reported in Ref. 11. In all cases, the frozen vibrational temperatures predicted by the finite-rate theory using this relation were hundreds of degrees higher than values measured spectroscopically, as shown in Table I. This verified the result reported in Ref. 11 and duplicated results found in several other laboratories (Refs. 10, 12, 13, and 14). It now seems to be well established, by three different experimental techniques, that vibrational rates obtained in shock experiments are not representative of the rates which prevail in rapidly expanding flows. Agreement of calculations and measured vibrational temperatures can be forced by simply increasing the vibrational rates (reducing the relaxation times of Eq. (2)) by the constant factors shown in Table I. These rate magnifications were found to vary from 4.4 to 28, depending on the reservoir condition.

The vibrational-relaxation time factor for N_2 (τ_p) is given as a function of static (translational) temperature in Fig. 12. The curve represented by Eq. (2) is shown, as well as some of the experimental data (from Ref. 11), by means of which the constants in Eq. (2) were derived. These are the shock-wave relaxation data. The reduced values of τ_p necessary to force agreement of experiment with theory in the present case are indicated by the shaded regions. These are compared with similar values obtained by a sodium-line reversal experiment in a pure N_2 expansion (Ref. 11) and with values obtained in an experiment similar to the present one (Ref. 13). The present results are in good agreement with Ref. 11 at high stagnation conditions but are generally higher than those of Ref. 13 at all temperatures. For the reservoir conditions of this investigation, the calculations showed little or no vibrational relaxation occurred at static temperatures below 1400°K. Thus, the low temperature differences in assumed τ_p between Refs. 11 and 13 and the present study have no effect on the resulting frozen vibrational temperatures.

It is noted that the data of Ref. 11 were for pure N_2 , whereas the present data were for air. In Ref. 13, data from both N_2 and air expansions were subjected to correlation by a single analytic function. It is shown theoretically in Refs. 33 through 35 that N_2 should relax more rapidly in air than in the pure state because of the presence of

atomic species and the exchange of vibrational energy with O_2 and NO . Theoretical values of τ_p for pure N_2 from Refs. 33 through 35 are given in Fig. 12. Theoretical values of τ_p for N_2 in an equilibrium air expansion lie between the correlation of Ref. 13 and the present data for the higher reservoir temperatures, indicating general agreement with the present experimental values. On the other hand, the lack of agreement between pure N_2 theory and the data of Ref. 11 cannot be explained at the present time.

5.2.2 Variables Other than Vibrational Temperature

The effect of nonequilibrium in an expanding flow will be manifested by many changes in the interrelationships between various thermodynamic variables. In the present case, there are four independent measured variables available for comparison with theory, since the vibrational temperature has already been used to infer the proper vibrational rate to use in the theory. These measurements may be compared with theory in many different ways, each having its own advantages and disadvantages. Two such methods are discussed below.

5.2.2.1 Graphical Comparisons

One common method compares one of the experimental measurements with theoretical values obtained at effective area ratios determined by the other measurements. Usually, the primary variable chosen for comparison has a large sensitivity to finite-rate effects, e. g., the static temperature. In Fig. 13a, b, and c, the static temperature is plotted versus area ratio for three different reservoir conditions selected to cover the complete range studied. These plots are simply enlarged segments of curves similar to those of Fig. 10. Theoretical finite-rate curves are given for both the normal and magnified vibrational rates, showing the relatively small effect of the vibrational rate on the static temperature. The experimental static temperature (N_2 rotational temperature) is plotted at "effective" area ratios extracted from the finite-rate solution at experimental values of static pressure, static density, and pitot pressure. The static pressure measurement was subjected to the corrections discussed in Section 4.4. The temperature data points represent the measurements as corrected by the empirical correction of Ref. 16, and the vertical bars extend upward to the uncorrected values.

It can be seen from these three plots that the magnitude of the finite-rate effect increases as stagnation temperature increases and that there is general agreement of measurements and calculations at each reservoir condition. This method of comparison of theory and experiment has

the advantage of economy of presentation (all four measured parameters entering into a single plot) and also gives a physical "feel" for the geometry of the flow. However, it has the distinct disadvantage that the comparison is not a strict experimental/theoretical comparison, since the abscissas of the experimental points are obtained by reference to specific finite-rate calculations. Of course, these points will converge on the theory in the limit of perfect accuracy of theory and measurement, but the "experimental" points in practical cases will contain some degree of theoretical bias inherent in the effective area ratios.

It is possible to compare measurements with theory in such a way that it is strictly experiment versus theory. In Figs. 14a, b, and c, static temperature is plotted versus static density. In this case, both coordinates of the experimental points are strictly experimental numbers, corrected where necessary (Section IV) but uninfluenced by any theoretical solution. This advantage is gained, however, at the expense of economy of presentation, since only two measured variables at a time can be compared with theory on such a two-dimensional basis. With four measured variables, a complete comparison with theory would require six separate plots such as those of Fig. 14 at each reservoir condition.

5.2.2.2 Numerical Comparison

To retain the purity of strictly experimental/theoretical comparison and yet avoid the complication of such a large number of plots, the complete experimental/theoretical comparison will be presented in numerical rather than graphical form. For this purpose, we define

$$R_{i,j} = \frac{(\text{experimental value of variable } i)}{\left(\begin{array}{c} \text{theoretical value of variable } i, \\ \text{at experimental value of variable } j \end{array} \right)} = \frac{v_{i\text{exp}}}{v_{i\text{theor}}(v_{j\text{exp}})} \quad (3)$$

In the formation of a given $R_{i,j}$, there are three sources of error: experimental error in v_i , experimental error in v_j , and error in converting from $v_{j\text{exp}}$ to $v_{i\text{theor}}$. It can be shown that, for small errors,

$$R_{i,j} = 1 + \epsilon_i - \left(\frac{v_j}{v_i} \frac{\partial v_i}{\partial v_j} \right) \epsilon_j - \epsilon_{\text{theor},i,j} \quad (4)$$

where the partial derivative is obtained at constant entropy in the expansion and the ϵ 's are percent errors. If we let

Subscript 1 refer to static temperature, T_1 ,

Subscript 2 refer to static pressure, p_1 ,

Subscript 3 refer to static density, ρ_1 , and

Subscript 4 refer to pitot pressure, p_{t2} ,

average values of the derivatives among these variables can be expressed as:

$$D_{i,j} = \begin{bmatrix} 1.0 & 0.29 & 0.40 & 0.40 \\ 3.5 & 1.0 & 1.4 & 1.4 \\ 2.5 & 0.72 & 1.0 & 1.0 \\ 2.5 & 0.72 & 1.0 & 1.0 \end{bmatrix} = \frac{v_j}{v_i} \frac{\partial v_i}{\partial v_j} = \frac{\partial \log v_i}{\partial \log v_j} \quad (5)$$

Because of the range in values of $D_{i,j}$, it is clear that errors in measurement of some variables will be contracted in the formation of $R_{i,j}$, whereas others will be magnified. Thus, there will likely be preferred combinations of variables for making the experimental/theoretical comparison.

In general, the errors, ϵ , will contain both systematic and random components. In an average of many $R_{i,j}$, the random components will disappear, and $\overline{R_{i,j}}$ will take the form of Eq. (4), in which the errors are only the systematic errors. In the present case, $R_{i,j}$'s were averaged over the ten reservoir conditions of Table I, and the resulting $(\overline{R_{i,j}})$'s are given in matrix form as:

$$(\overline{R_{i,j}}) = \begin{bmatrix} x & 1.040 & 0.975 & 1.074 \\ 0.880 & x & 0.810 & 1.146 \\ 1.075 & 1.187 & x & 1.279 \\ 0.840 & 0.950 & 0.790 & x \end{bmatrix} \quad (6)$$

This matrix then represents the complete experimental/theoretical comparison averaged over the ten reservoir conditions. Before averaging, the elements symmetrically disposed around the diagonal of the $R_{i,j}$ matrix are simply related to each other. In general, however, the elements of $\overline{R_{i,j}}$ are not so related, and the complete comparison requires all 12 components. It can be seen that the agreement of measurements with theory ranges from within -21 percent for R_{p_{t2}, ρ_1} to within

+28 percent for R_{p_1, p_2} . Although the individual $\overline{R_{i,j}}$ range over these rather wide limits, the overall average of $\overline{R_{i,j}}$ is close to unity,

$$\overline{(\overline{R_{i,j}})} = 1.004 \quad (7)$$

As anticipated by observation of Eq. (4) and the matrix of derivatives, Eq. (5), there are preferred combinations of variables. The values of $(\overline{R_{i,j}}) - 1$ are not simply proportional to values of $D_{i,j}$, because the individual errors are not the same for all variables. However, a certain similarity between $[(\overline{R_{i,j}}) - 1]$ and $D_{i,j}$ can be observed. Obviously, combinations of variables which use static temperature as the primary variable of comparison, $(\overline{R_{T_1,j}})$, are very desirable, and this could almost be predicted from the form of $D_{i,j}$. Conversely, the $(\overline{R_{i,T_1}})$ which use T_1 to define the theoretical value of some primary variable of comparison are quite poor.

Whether a given combination attains a high quality by virtue of small values of the errors, ϵ , or by favorable values of the derivatives, $D_{i,j}$, it is naturally advantageous to focus attention on the best of these combinations. The $\overline{R_{i,j}}$ which use static temperature as the primary variable of comparison — that is, the first row of the $\overline{R_{i,j}}$ matrix — are displayed in bar chart form as $(\overline{R_{T_1,j}} - 1)$ in Fig. 15. Values of $(\overline{R_{T_1,j}} - 1)$ from other matrixes are also shown, namely for the case where normal vibrational rates are used in the theory and also for the case where the uncorrected measured temperature was used.

Certain general conclusions concerning the agreement of measurements and theory can be made by observation of Fig. 15:

1. The uncorrected static temperatures are badly in error in comparison with those corrected by the empirical correction of Ref. 16.
2. The magnified vibrational rates give a generally better experimental/theoretical agreement than do the normal rates. This is not true for some of the components of $\overline{R_{i,j}}$ which are not shown in Fig. 15, but, on the average, it is true for the entire matrix. It is sufficiently significant here that the magnified rates merely do not disagree with experiment, since the overriding justification for the magnified rates is not the static (translational) temperature but the measured vibrational temperature.

3. In absolute terms, the best correlation of experiment and theory is given by the ratio $(\overline{RT_1}, \rho_1)$, 2.5 percent. It is considered significant, in this connection, that T_1 and ρ_1 are the only experimental variables which share the two characteristics of being measured at precisely the same location in the flow, which eliminates need for geometric corrections, and being measured without introduction of gross aerodynamic disturbances in the flow.

5.3 GENERAL CORRELATION OF FINITE-RATE EFFECTS IN NOZZLE EXPANSION

The experimental/theoretical comparisons discussed in Section 5.2.2 are all based on absolute values of various parameters, no reference being made to the magnitude of effects produced by nonequilibrium in the flow. In this section, the comparison of theory and experiment is examined from the standpoint of the magnitude of the finite-rate effects, which will be specified by parameters of the form,

$$\frac{v_i}{v_{iEQ}}$$

where v_i may be either an experimental measurement or a calculated value, and v_{iEQ} is the value of v_i in an equilibrium expansion.

It is also of interest to examine the possibility of a general correlation of the finite-rate effect, rather than simply isolated presentation of v_i/v_{iEQ} at separate reservoir conditions. It was observed a number of years ago (Refs. 21 and 22) that there were a number of nonequilibrium flow phenomena in calculated expansions which correlated very simply with the reservoir entropy, S_{t1}/R . A further remarkable correlation was recently reported in Ref. 36, in which the entropy parameter was supplemented by a rate parameter, τ_c . This rate parameter was derived for a nonequilibrium flow at constant velocity, which is approximated by flow in a supersonic nozzle downstream of the throat region. This parameter was not useful in the present experiment, however, because reservoir conditions were such that the nonequilibrium began upstream of the nozzle throat where there were large variations in the flow velocity (Fig. 11). Instead, the Σ parameter of Ref. 37, which contains both reservoir entropy and nozzle scale, was used:

$$\Sigma = \frac{S_{t1}}{R} + 0.4 \ln \left(\frac{\tan \theta}{r^*} \right) \quad (8)$$

In this relation, r^* is expressed in inches. In Fig. 16a, the finite-rate effect on static temperature, expressed as T_1/T_{1EQ} , is plotted versus Σ

for the range of reservoir conditions covered in Table I. The experimental points represent the static temperature measured at each reservoir condition divided by static temperature in an equilibrium expansion at points determined separately by measured values of ρ_1 , p_1 , and P_{t2} . Also, the T_1/T_{1EQ} ratios from the finite-rate theory were all taken at constant density in order that the theoretical solutions would be reduced to a single curve for comparison with the measurements. Naturally, the finite-rate theory with magnified vibrational rates and the best (corrected) experimental values were used as a basis for this comparison.

A clearly defined trend of the theoretical finite-rate effect can be seen in Fig. 16a, and the experimental data agree with this trend over the complete range of the Σ parameter covered. The finite-rate effect appears to be negligible for $\Sigma < 26.0$, but the theoretical reduction in static temperature caused by the nonequilibrium withholding of chemical and thermal energy from the flow reaches 85 percent at $\Sigma \approx 37.0$. Experimentally, this reduction is found to be 85.3 to 87.2 percent, depending on the measurement used to define the point in the expansion. In terms of absolute temperature differences, the maximum theoretical finite-rate effect on temperature is a 780°K decrease, and the measured decrease is 792°K, based on measured density. As noted previously, the T_1, ρ_1 combination does not uniformly give the best agreement of theory and experiment at each individual reservoir condition but averaged over all reservoir conditions it does.

In Fig. 16b, the finite-rate effect on static pressure is presented as a function of Σ in the same way as for temperature in Fig. 16a. Although there are reservations about the accuracy of the (corrected) static pressure measurements, it is considered instructive to make this correlation because the static pressure is nearly as sensitive to finite-rate flow effects as is the static temperature. As with temperature, there is a regular downward trend of theoretical P_1/P_{1EQ} as Σ increases. There is also observable a fair agreement of the experimental measurements with this trend, at least in the range $29 < \Sigma < 34$. The relatively larger scatter of the P_1/P_{1EQ} points defined by the other measurements is, of course, related to the inherent error-magnifying effect of the large derivative of static pressure with respect to all other variables, i. e., the second row of $D_{i,j}$, Eq. (5).

5.4 RESULTS OF THEORETICAL/EXPERIMENTAL AGREEMENT

5.4.1 General Inferences

It seems to have been demonstrated reasonably well (Figs. 13 through 16) that the static temperature in a nonequilibrium flow is accurately measurable by the electron-beam technique and that the measurements agree with finite-rate expansion calculations to a very satisfactory degree. At various stages of development of finite-rate expansion theories, experimental verification has been desired to assure that the chemical-kinetic formulation used was adequate under conditions of rapid expansions and also that the basic characteristic rate constants of various reactions were reasonably accurate. The present results represent a further contribution to the growing confirmation of these theories by virtue of, first, measurement of that thermodynamic variable which is most sensitive to nonequilibrium and, second, a large enough range in reservoir conditions that a general correlation of the nonequilibrium effects is demonstrated. For quite some time, there has been no doubt that the reaction kinetics itself was properly represented, but the accuracy of the basic rate data has been under question. The present experiments confirm the current belief that vibrational de-excitation rates which prevail in rapid expansions must be determined in such flows and cannot be inferred from vibrational excitation rates observed in shock-type flows. This fundamental difference between vibrational rates in compression and expansion flows was determined specifically only for N_2 , but similar results have been found for CO (Ref. 14), and it is very likely that the same situation prevails for O_2 and NO . On the other hand, the chemical reaction rate data, which have been mainly obtained in shock experiments, appear to be entirely valid in rapid expansions.

Although the present work represents a positive step in the verification of finite-rate flow expansion theory, it is far from complete. Ideally, at least three more features would be required. First, verification should be extended to such a range in reservoir conditions that a complete transition from equilibrium to fully frozen flow could be measured. Second, the verification should be completed in the exact sense by performing measurements of composition in the flowing gas. Third, a direct verification of theory would be desirable in the precise regions of flow in which the nonequilibrium disturbance is generated, i. e., at small area ratios near the nozzle throat. The first two of these ideal requirements appear to be quite possible. However, it is doubtful that the third requirement will ever be met because of the very large gradients of all flow properties and the severe environment near the nozzle throat.

The fact that thermodynamic variables measurable at large area ratios are evidently predictable by finite-rate theory is quite strongly suggestive that this theory is actually closely representative of the flow in those regions where finite-rate conditions occur near the throat. The reason for this is that the flow downstream of the (limited) finite-rate region is at constant composition with a constant specific heat ratio defined by the frozen composition ($\gamma > 1.4$ because of the frozen monatomic species). The thermodynamics of such flows is especially simple and well known; the $\gamma = 1.4$ isentropic expansion in a conventional wind tunnel nozzle is the most familiar example of such a flow. Except for a small amount of curvature at $A/A^* \leq 10$ (Fig. 10), the curve of T versus A/A^* is a straight line on logarithmic coordinates and can be shown to have a slope of $(1 - \gamma)$. Extension of such curves in either direction over large ranges in area ratio is very simple and has a sound theoretical basis. Hence, the good agreement of measurement and theory at large area ratios is inferred to indicate the flow solutions are valid at the beginning of the frozen flow region at low area ratios.

5.4.2 Routine Flow Calibration of Nonequilibrium Flows

The direct proof that thermodynamic variables at large area ratios are predictable by finite-rate expansion theory (and indirect inference that the same is true at low area ratios) provides a basis for performing routine calibration of high enthalpy nozzle expansions which depart from equilibrium. The diagnostic procedure can be entirely similar to that used in conventional wind tunnel practice and will differ only in the theoretical formulation of the thermodynamics of the expansion process. The following steps will be included:

1. Precise determination of the state of the gas in the stagnation reservoir. If the reservoir is adequately sized, the gas will be in equilibrium at this point, and its state can be determined by measurement of any two thermodynamic variables. Reservoir pressure is almost always one of these measurements, and the reservoir temperature or enthalpy is the other. In most arc-heated facilities, this means accurate energy-balance measurements.
2. Analytical formulation of the finite-rate thermodynamic processes in the nozzle expansion by the theory described in Section 5.1. The complexity of the thermodynamic properties at high temperature and the addition of the expansion rate as an important flow parameter dictate that a separate calculation is required for each reservoir condition and nozzle size. Nevertheless, these calculations are the exact analogue of the

$\gamma = 1.4$ compressible flow tables used in conventional wind tunnel work independent of the nozzle scale or supply condition.

3. Measurement of a single convenient parameter at some point of interest in the expanded flow to locate this point in the theoretical calculation. The values of the other flow variables at that point are thus defined. The remarks made in Section 5.2.2 concerning the desirability of various parameters for determination of effective area ratio apply only to the very special conditions of this investigation, namely, a flow-model validation study performed at very low densities. It is not foreseen, for example, that the static density measurement will become a routine measurement for flow calibration nor do the nonequilibrium limitations on pitot pressure apply generally at higher densities. It is probable that the pitot pressure and the static pressure will continue to be the variables most suited to routine calibration of high enthalpy flows.

The requirement of a separate and distinct finite-rate flow calculation for each specific nozzle expansion is likely to prove very burdensome in wind tunnel work. The work of Ref. 36 has pointed the way to a means of systematizing the results of many such calculations so that something approaching the simplicity of constant- γ isentropic flow tables may be possible even for highly nonequilibrium flows.

SECTION VI CONCLUSIONS

1. A systematic study of experimental measurements in high enthalpy nonequilibrium nozzle flows of air has revealed very good agreement with conditions predicted by finite-rate expansion calculations for the specific nozzle geometry and reservoir conditions in the range from 5 to 20 atm of pressure and temperatures from 2300 to 5000°K. The theoretical/experimental comparison was primarily in terms of the static temperature measured by the electron-beam probe technique. The flow expansion used a slightly simplified air model and allowed for finite-rate chemical reactions and simultaneous (but uncoupled) finite-rate vibrational energy exchanges.
2. Vibrational temperatures measured by the electron-beam probe were hundreds of degrees lower than values predicted using vibrational rates obtained in shock-tube experiments. The measured values corresponded to vibrational rates 4 to 28 times

more rapid than the shock tube rates, which is in general agreement with several other reported experiments. Apparently, vibrational deexcitation rates to be used in expansion flow calculations must be obtained in experiments on expanding flows.

3. Vibrational-rate magnifications of up to 28x were found to have only small effects on the calculated static translational temperatures in a flow, but on the average, these small effects were in the direction of better agreement with the measurements. The generally good agreement of the static temperatures implies that the chemical reaction rate data used in the calculations were accurate.
4. A general correlation of the nonequilibrium effects on static temperature and pressure in the expansions was obtained for the entire range of operating conditions, using a correlating parameter which was dependent mainly on reservoir entropy.
5. The excellent experimental/theoretical agreement found at large area ratios was interpreted as indirect verification of nonequilibrium flow solutions at small area ratios because of the inherent simplicity of the frozen, constant- γ flow downstream of the regions in the nozzle in which finite-rate conditions actually prevail. The finite-rate theory can thus provide the basis for routine calibration of high enthalpy, nonequilibrium nozzle expansions at all area ratios.
6. The electron-beam techniques for measuring static temperature and static density were found to be very valuable tools for purposes of validation of the flow theory. In fact, for the special conditions under which this investigation was made, the density and temperature were found to be the best combination of experimental measurements for demonstrating the validity of the theory. For purposes of routine flow calibration, however, it is likely that the static and pitot pressures will remain as the most convenient measurements.
7. Evidence was found in the experimental measurements that the formal Muntz theory of electron-beam excitation and emission is not completely accurate and requires a small empirical correction. In the temperature range of interest in the present study, this correction is approximately 8 percent of the measured rotational temperature.
8. The present experiment represents the first comprehensive test of the density measurement by counting of electrons scattered out of the electron beam. The repeatability obtained

was ± 10 percent. This technique is considered very promising because it does appear capable of further refinement, and it has the unique capability of measuring the mass density independent of the degree of dissociation of the scattering particles.

REFERENCES

1. Hilsenrath, J. and Klein, M. "Tables of Thermodynamic Properties of Air in Chemical Equilibrium Including Second Virial Corrections from 1500°K to 15,000°K." AEDC-TR-65-58 (AD612301), March 1965.
2. Penner, S. S. Introduction to the Study of Chemical Reactions in Flow Systems. Butterworths Scientific Publications, Ltd., London, 1955.
3. Bray, K. N. C. "Atomic Recombination in a Hypersonic Wind-Tunnel Nozzle." Journal of Fluid Mechanics, Vol. 6, 1959, pp. 1-32.
4. Eschenroeder, A. Q., Boyer, D. W., and Hall, J. G. "Exact Solutions for Nonequilibrium Expansions of Air with Coupled Chemical Reactions." Cornell Aeronautical Laboratory Report AF-1413-A-1, May 1961.
5. Emanuel, G. and Vincenti, W. G. "Method for Calculation of the One-Dimensional Nonequilibrium Flow of a General Gas Mixture through a Hypersonic Nozzle." AEDC-TDR-62-131 (AD276822), June 1962.
6. Levinsky, E. S. and Brainerd, J. J. "Inviscid and Viscous Hypersonic Nozzle Flow with Finite Rate Chemical Reactions." AEDC-TDR-63-18 (AD293448), January 1963.
7. Nagamatsu, H. T. and Sheer, R. E. "Vibrational Relaxation and Recombination of Nitrogen and Air in Hypersonic Nozzle Flows." AIAA Journal, Vol. 3, 1964, pp. 1386-1391.
8. Duffy, R. E. "Experimental Study of Nonequilibrium Expanding Flows." AIAA Journal, Vol. 3, 1965, pp. 237-244.
9. Sebach, D. I. and Duckett, R. J. "A Spectrographic Analysis of a 1-Foot Hypersonic-Arc-Tunnel Airstream Using an Electron Beam Probe." NASA TR-R-214, December 1964.
10. Petrie, S. L., Pierce, G. A., and Fishburne, E. S. "Analysis of the Thermo-Chemical State of an Expanded Air Plasma." USAF FDL-TR-64-191, August 1965.

11. Hurle, I. R., Russo, A. L., and Hall, J. G. "Spectroscopic Studies of Vibrational Nonequilibrium in Supersonic Nozzle Flows." USAF ARL-65-6, January 1965.
12. Cunningham, J. W., Fisher, C. H., and Price, L. L. "Measurement of Local Density and Temperature in Wind Tunnels Using Electron Beams." IEEE Transactions on Aerospace and Electronic Systems, Vol. AES-3, No. 2, March 1967.
13. Sebacher, D. I. "A Correlation of N₂ Vibrational→Translational Relaxation Times." AIAA Journal, Technical Note, Vol. 5, No. 4, April 1967, pp. 819-820.
14. Russo, A. L. "Spectrophotometric Measurements of the Vibrational Relaxation of CO in Shock Wave and Nozzle Expansion — Flow Environments." Cornell Aeronautical Laboratory, Report No. AD-1689-A-8, July 1967.
15. Muntz, E. P. "Measurement of Rotational Temperature, Vibrational Temperature, and Molecular Concentration, in Non-Radiating Flows of Low Density Nitrogen." University of Toronto Institute Aerophysics Report No. 71 (AFOSR-TN-60-499), April 1961.
16. Robben, F. and Talbot, L. "Some Measurements of Rotational Temperatures in a Low Density Wind Tunnel Using Electron Beam Fluorescence." University of California Report No. AS-65-5 (AD466305), May 1965.
17. Marrone, P. V. "Rotational Temperature and Density Measurements in Underexpanded Jets and Shock Waves Using an Electron Beam Probe." University of Toronto Institute Aerospace Studies, UTIAS Report No. 113, April 1966.
18. Schumaker, B. W. and Gadamer, E. O. Canadian Journal of Physics, Vol. 36, 1958, pp. 659-671.
19. Cunningham, J. W. and Fisher, C. H. "Measurement of Gas Density by Electron Scattering." AEDC-TR-66-212 (AD646590), February 1967.
20. Ashkenas, H. "Rotational Temperature Measurements in Electron-Beam Excited Nitrogen." Physics of Fluids, Vol. 10, No. 12, December 1967, p. 2504.
21. Harris, C. J. and Warren, W. R. "Correlation of Nonequilibrium Chemical Properties of Expanding Air Flows." General Electric MSD R64SD92 (AD621857), December 1964.

22. Bray, K. N. C. "A Simplified Sudden-Freezing Analysis for Non-equilibrium Nozzle Flows." University of Southampton, A.A.S.U. Report No. 161 (AD267108), December 1960.
23. Potter, J. L., Kinslow, M., and Boylan, D. E. "An Influence of the Orifice on Measured Pressures in Rarefied Flow." AEDC-TDR-64-175 (AD447734), September 1964.
24. MacDermott, W. N., Dix, R. E., and Shepard, J. E. "High Temperature, Low Density Boundary-Layer Control by Cryogenic Pumping." AEDC-TR-66-177 (AD634963), December 1966.
25. Guy, R. W. and Winebarger, R. M. "Effect of Orifice Size and Heat-Transfer Rate on Measured Static Pressures in a Low-Density Arc-Heated Wind Tunnel." NASA TN D-3829, February 1967.
26. Lordi, J. A., Mates, R. E., and Moselle, J. R. "Computer Program for the Numerical Solution of Nonequilibrium Expansions of Reacting Gas Mixtures." Cornell Aeronautical Laboratory, Inc., Report No. AD-1689-A-6, October 1965.
27. Gavril, Bruce D. "Generalized One-Dimensional Chemically Reacting Flows with Molecular Vibrational Relaxation." General Applied Science Laboratories, Inc., TR 426 (AD435623), January 1964.
28. Mates, R. E. and Lordi, J. A. "Techniques for Solving Non-equilibrium Expanding Flow Problems." Cornell Aeronautical Laboratory, Inc., Report No. ARL 65-2, January 1965.
29. Treanor, C. E. and Marrone, P. V. "Effect of Dissociation on the Rate of Vibrational Relaxation." Physics of Fluids, Vol. 5, No. 9, September 1962, pp. 1022-1026.
30. Treanor, C. E. "A Method for the Numerical Integration of Coupled First Order Differential Equations with Greatly Different Time Constants." Cornell Aeronautical Laboratory, Inc., Report No. AG-1729-A-4, January 1964.
31. Lomax, Harvard and Bailey, Harry E. "A Critical Analysis of Various Numerical Integration Methods for Computing the Flow of a Gas in Chemical Nonequilibrium." NASA TN-D4109, August 1967.
32. Dix, R. E. "Sampling Probe for Instantaneous Mass Spectrometric Analysis of Rarefied High Enthalpy Flow." AEDC-TR-69-37, March 1969.

33. Schwartz, R. N., Slawsky, Z. I., and Herzfeld, K. F. "Calculation of Vibrational Relaxation Times in Gases." Journal of Chemical Physics, Vol. 20, 1952, p. 1591.
34. Schwartz, R. N. and Herzfeld, K. F. "Vibrational Relaxation Times in Gases (Three Dimensional Treatment)." Journal of Chemical Physics, Vol. 22, 1954, p. 767.
35. Tanczos, F. I. "Calculation of Vibrational Relaxation Times of the Chloromethanes." Journal of Chemical Physics, Vol. 25, 1956, p. 439.
36. Ring, L. E. and Johnson, P. W. "Correlation and Prediction of Air Non-Equilibrium in Nozzles." AIAA Paper No. 68-378, AIAA 3rd Aerodynamic Testing Conference, San Francisco, April 8-10, 1968.
37. Harney, D. J. "Similarity of Nonequilibrium Air Expansions in Hypersonic Nozzles." USAF FDL-TM-67-1 (AD664084), May 1967.
38. Hickman, R. S. "Rotational Temperature Measurement in Nitrogen Using an Electron Beam." AFOSR 66-2509; also University of Southern California USCAE 104, September 1966.
39. Hunter, W. W. "Investigation of Temperature Measurements in 300° to 1100°K Low-Density Air Using an Electron Beam Probe." NASA TN D-4500, May 1968.
40. Williams, W. D. "Laboratory Verification Studies of Rotational and Vibrational Temperature Measurements by the Electron Beam Technique." AEDC-TR-68-265 (AD683001), February 1969.

APPENDIXES

- I. ILLUSTRATIONS**
- II. TABLES**
- III. TEMPERATURE MEASUREMENTS BY THE ELECTRON-BEAM TECHNIQUE**
- IV. DETERMINATION OF DENSITY BY ELECTRON BEAM**

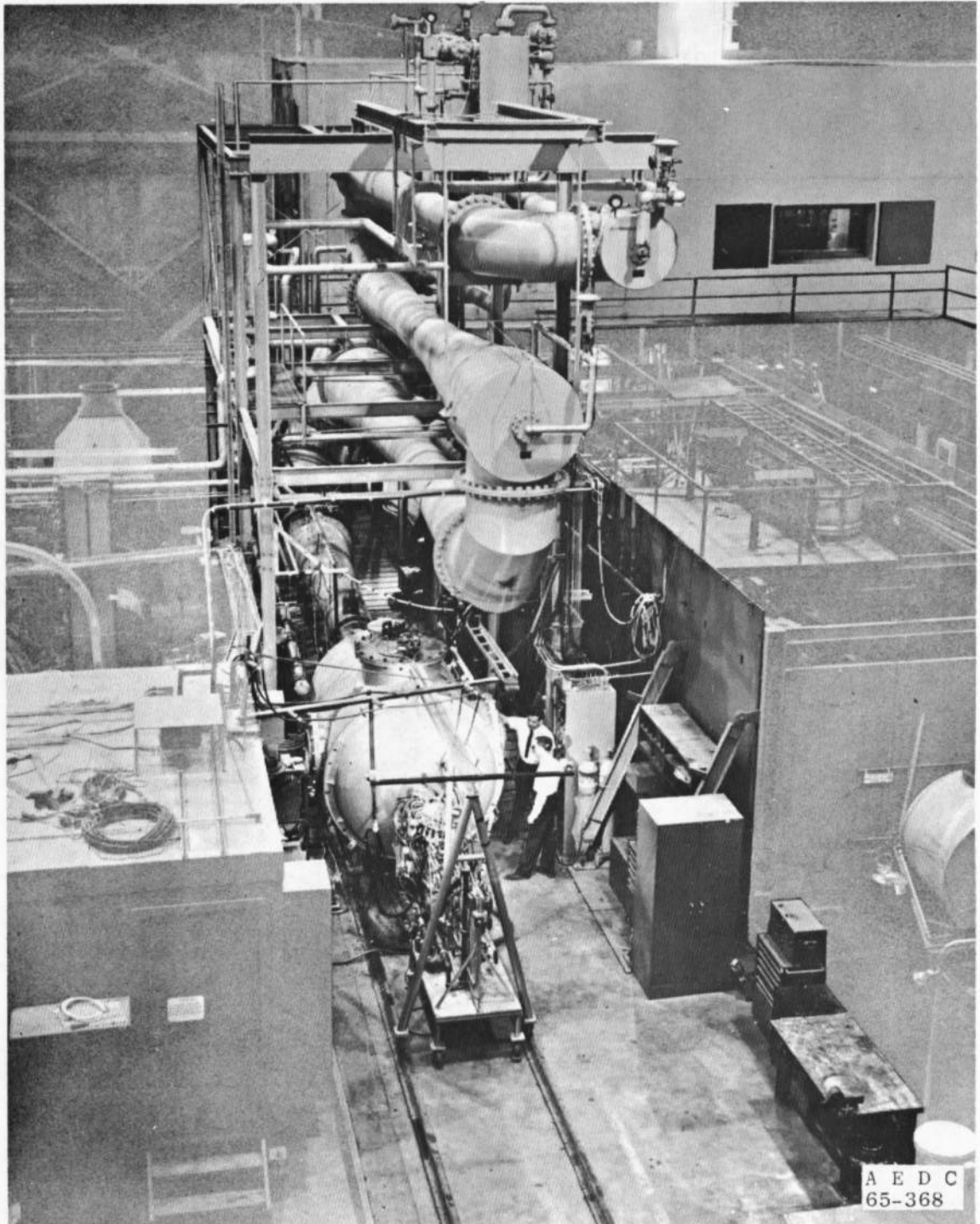


Fig. 1 Photograph of the 18-in. Hypersonic Wind Tunnel

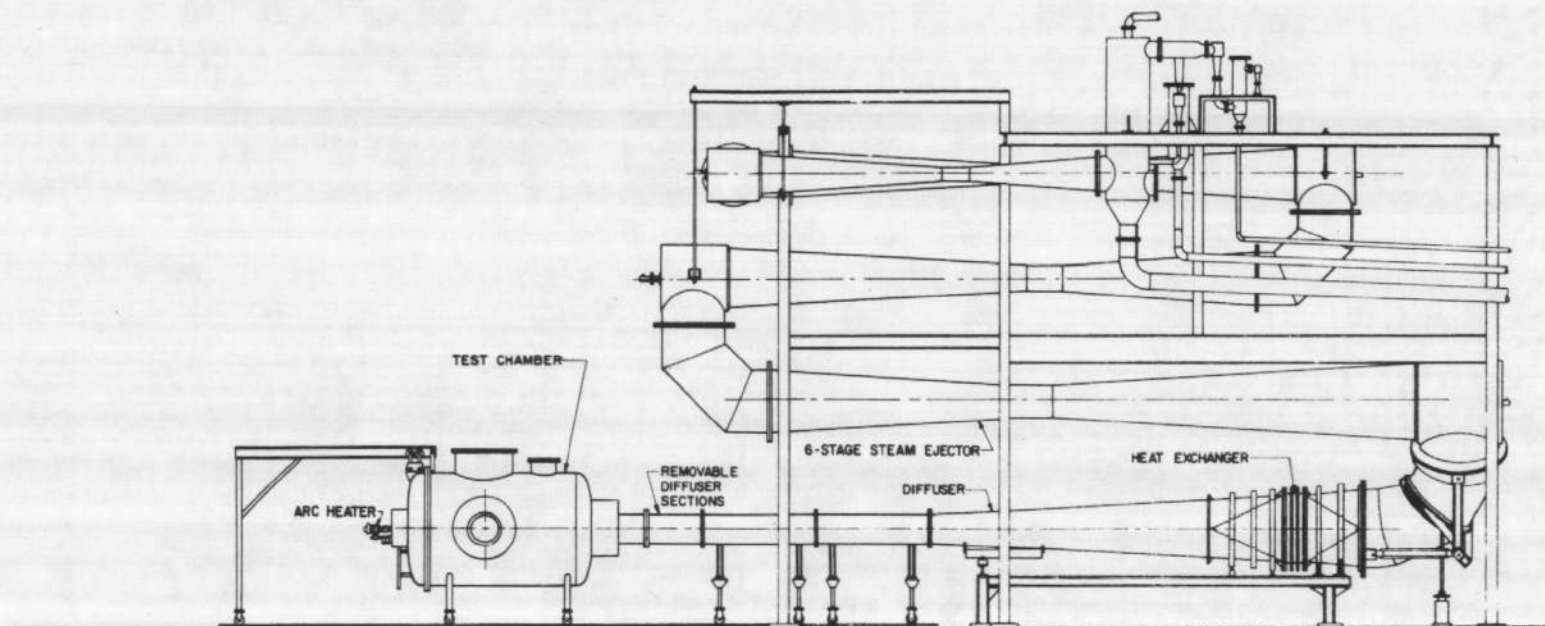


Fig. 2 Sketch of the 18-in. Hypersonic Wind Tunnel

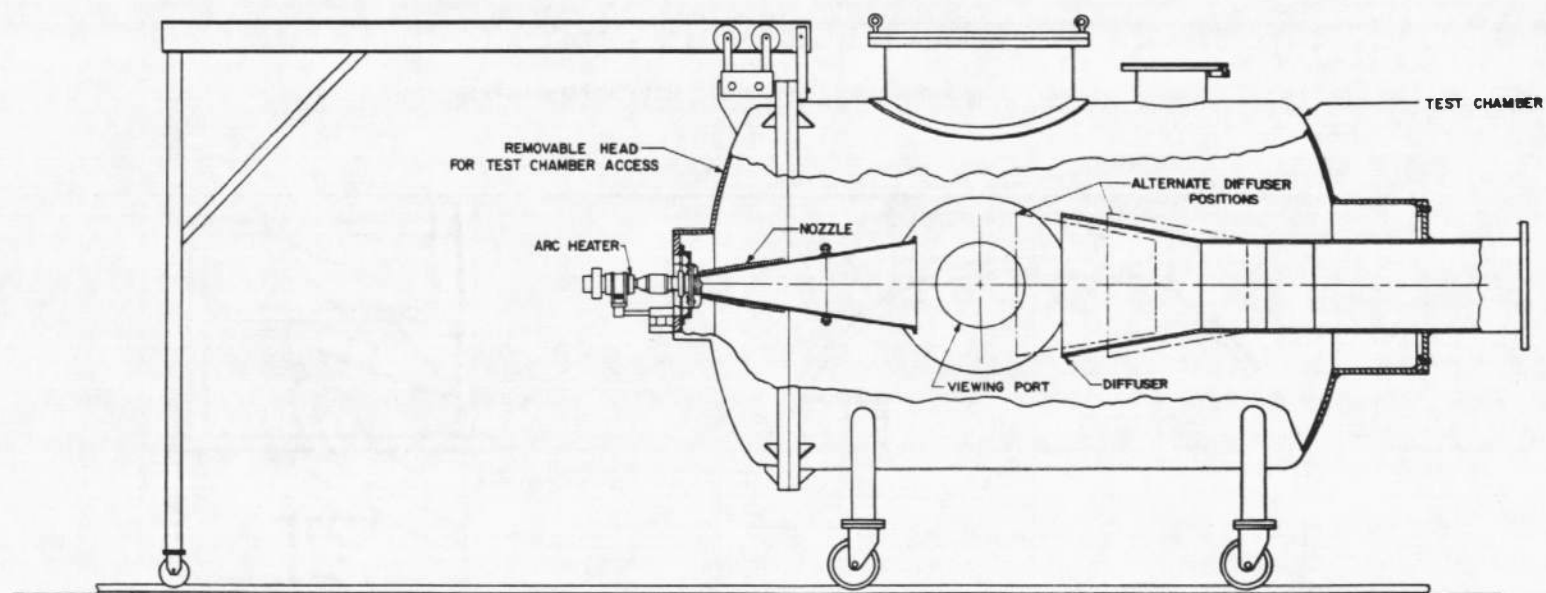
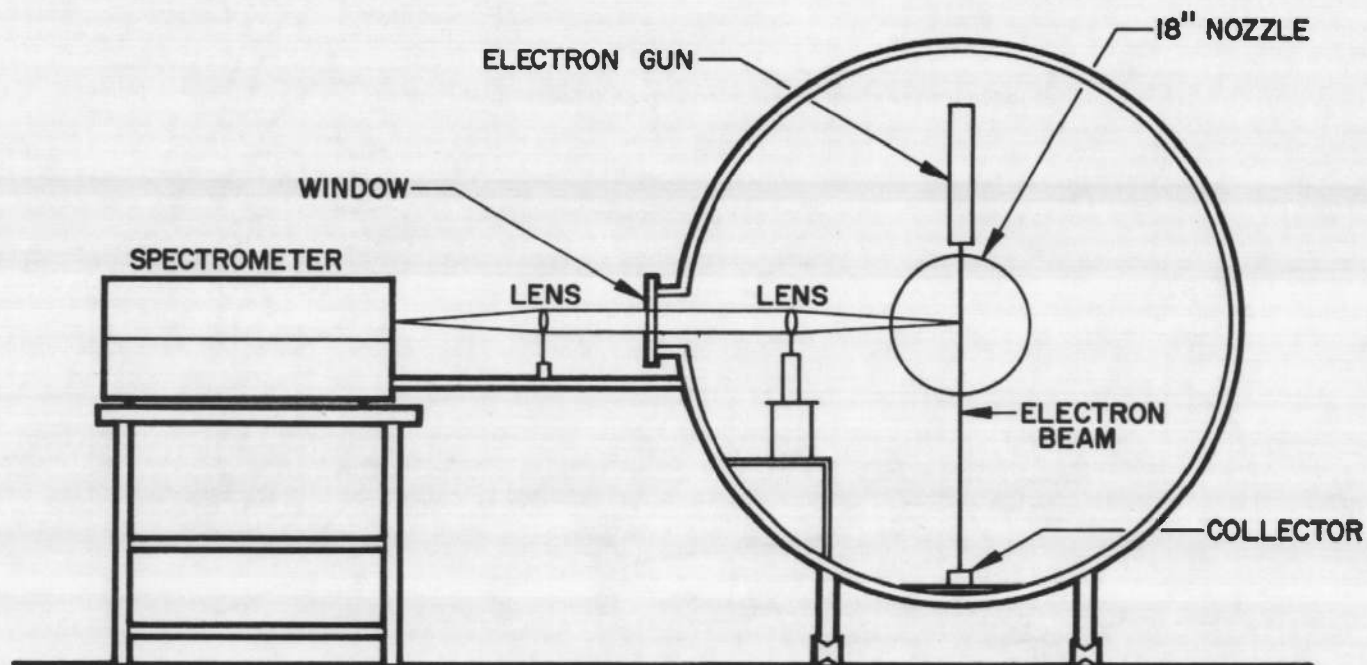
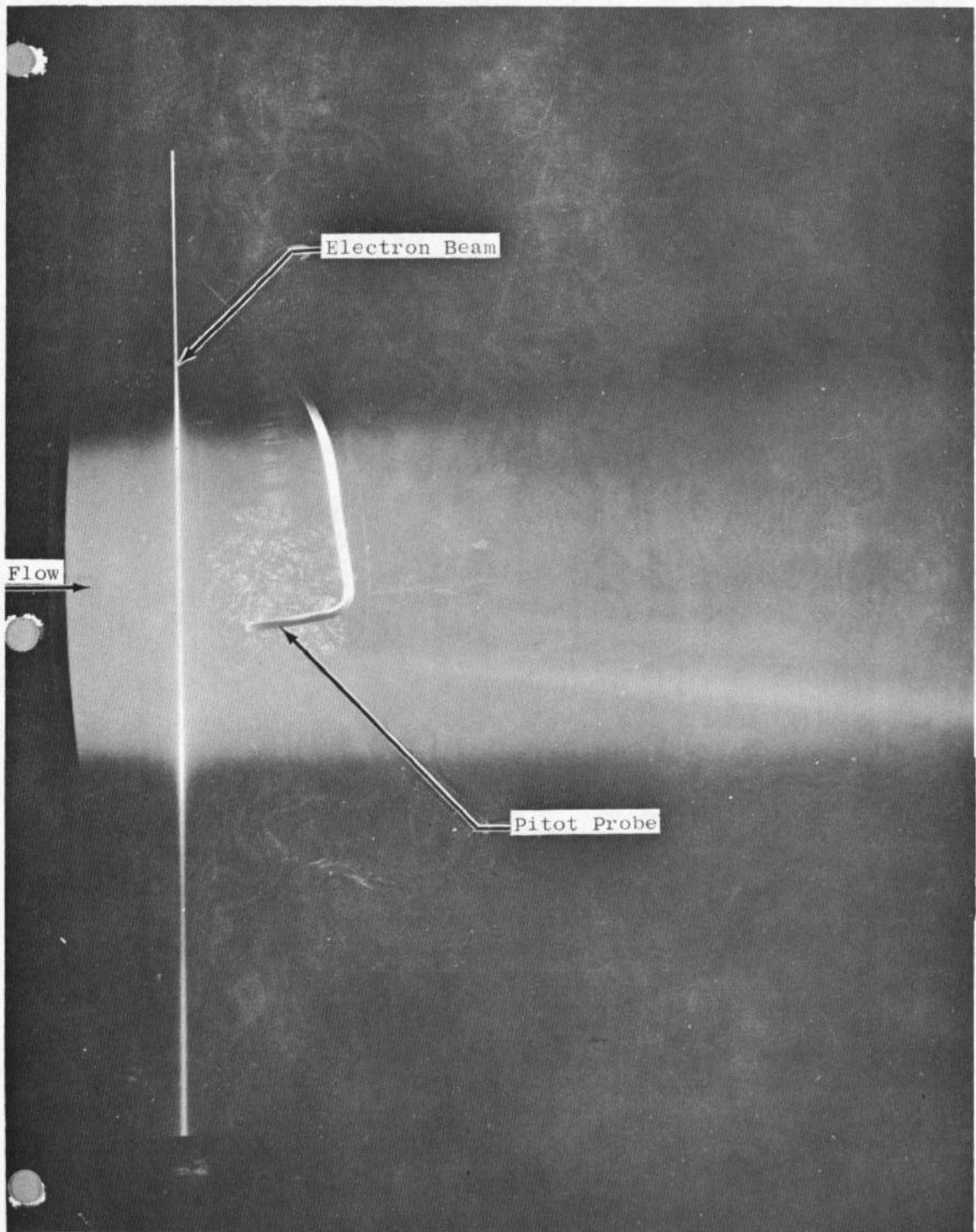


Fig. 3 Arrangement of Components in the Test Chamber



a. Electron-Beam Installation for Temperature Measurement

Fig. 4 Electron-Beam Installation



b. Photograph of Flow with Electron Beam Used for Temperature Measurement
Fig. 4 Concluded

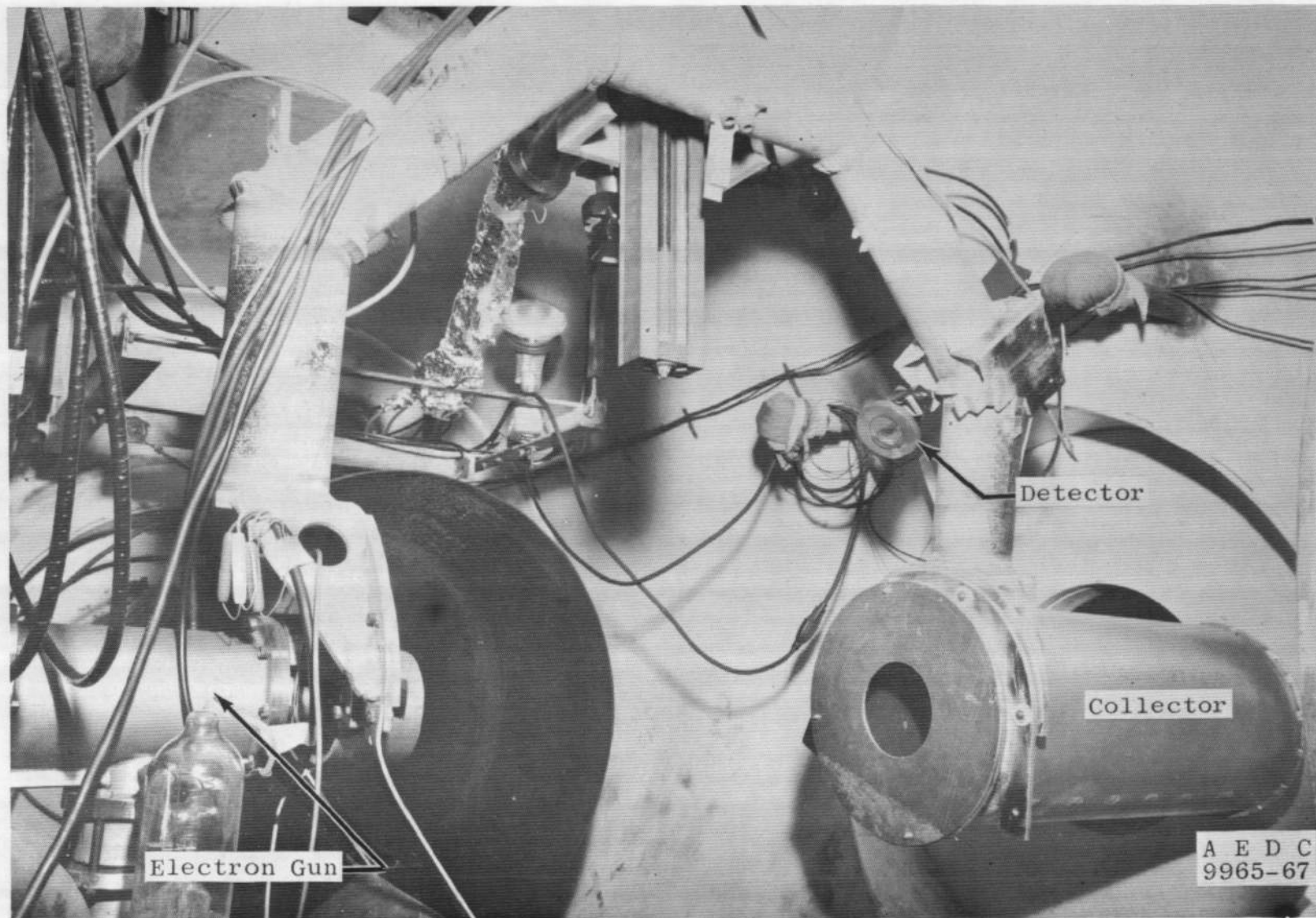


Fig. 5 Electron-Beam Installation for Density Measurement

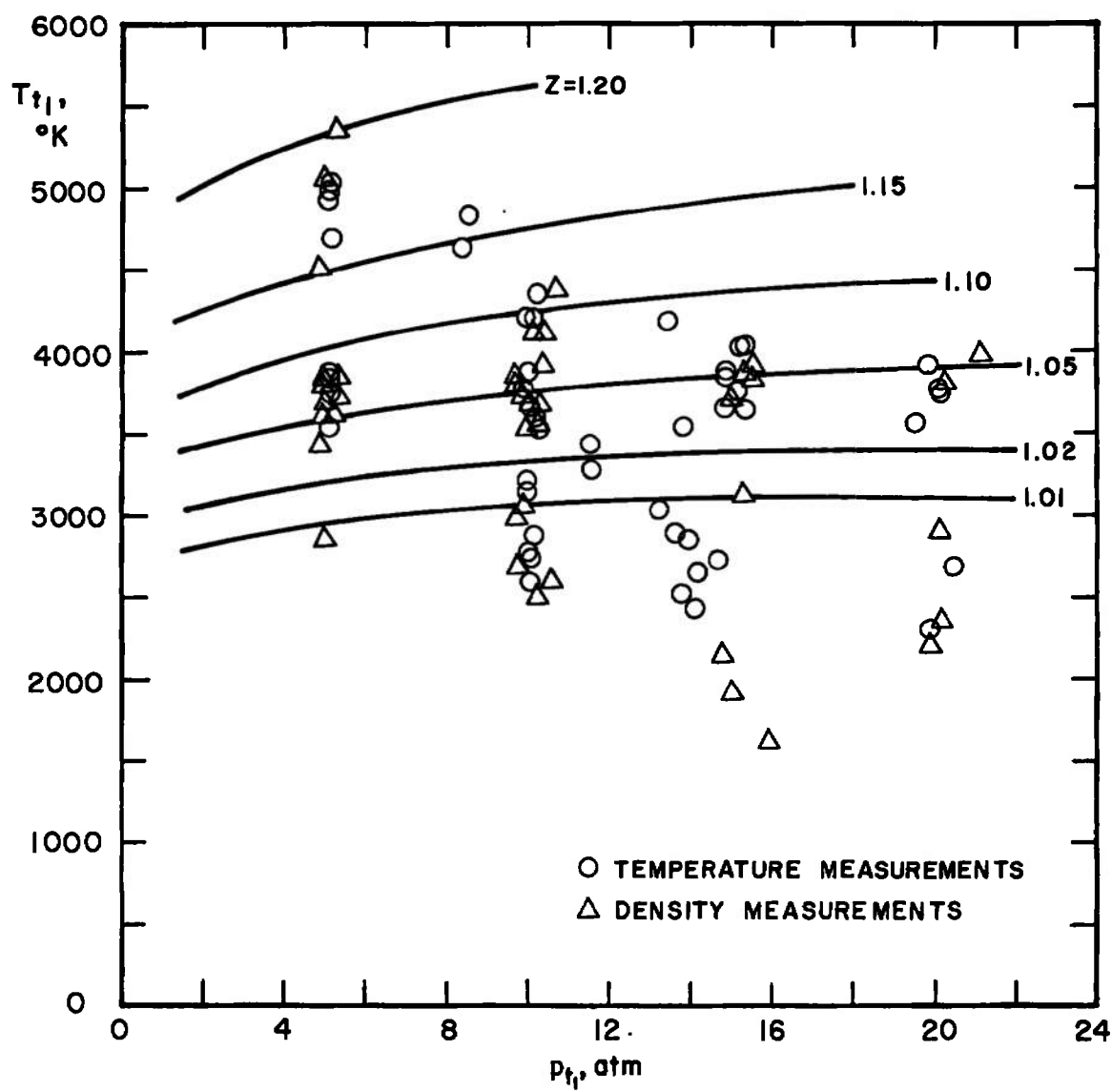


Fig. 6 Reservoir Conditions for Individual Runs

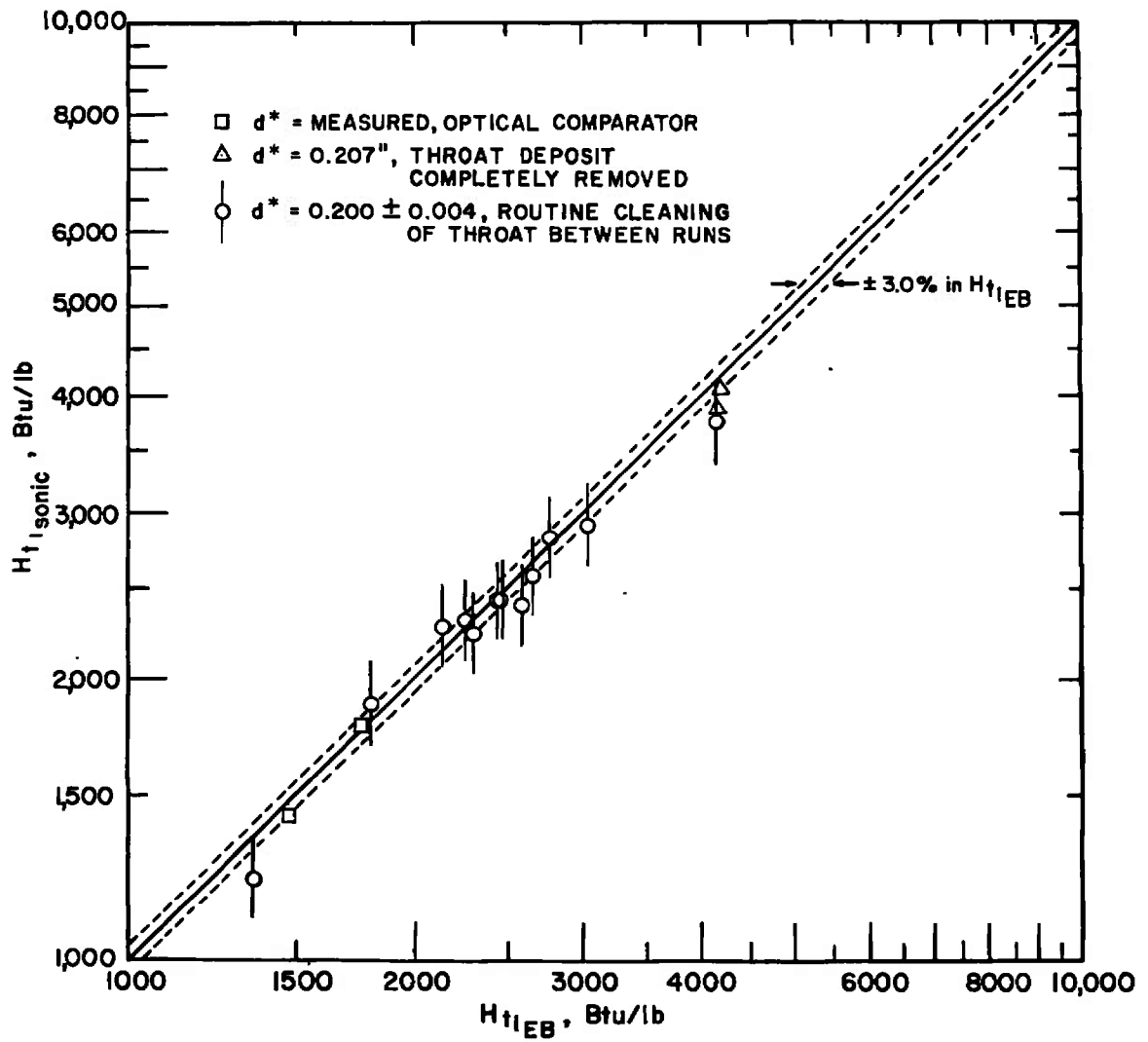


Fig. 7 Comparison of Total Enthalpy from Energy Balance and Sonic Flow Calculation

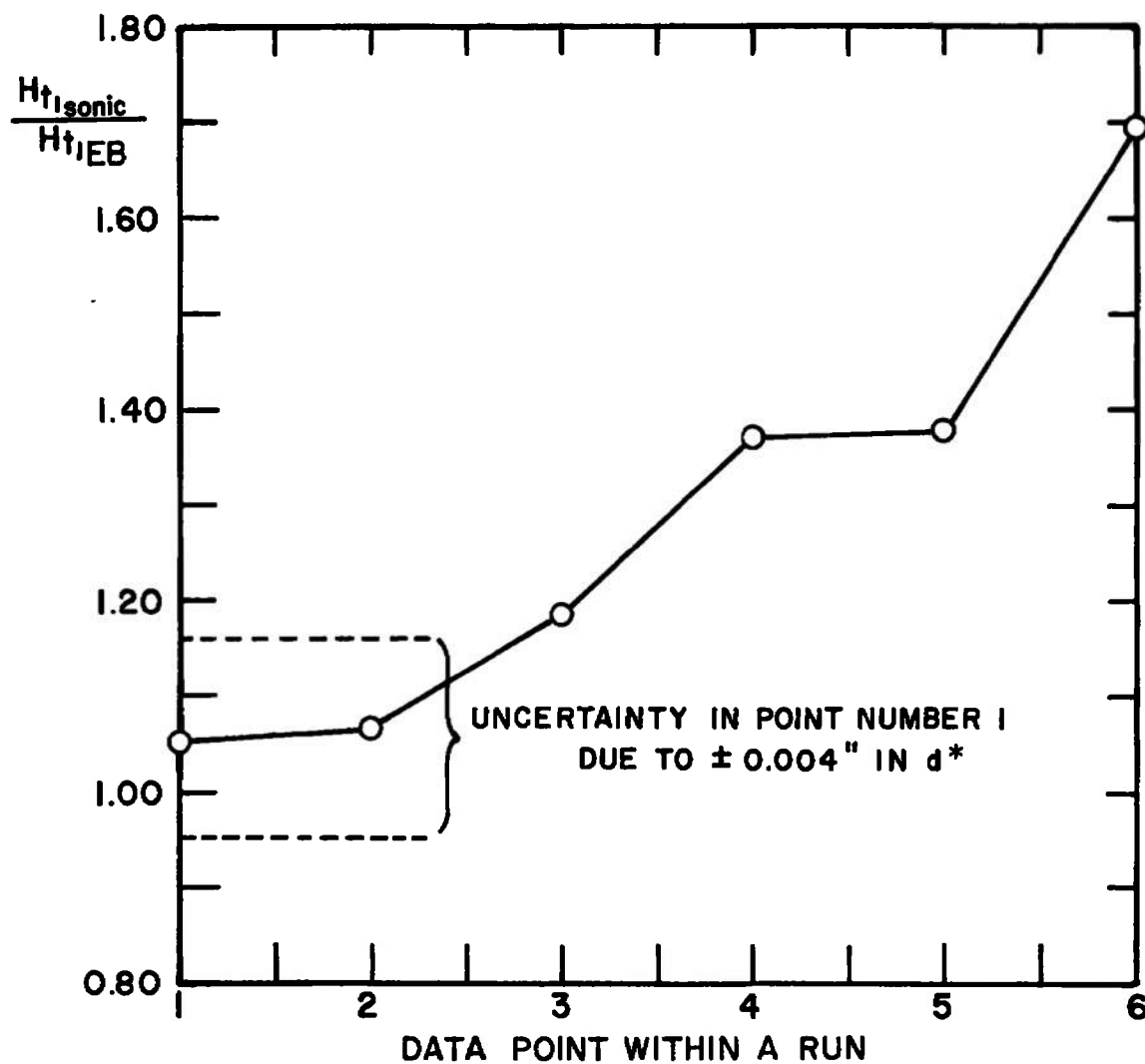


Fig. 8 Effect of Throat Contamination on Indicated Sonic Flow Enthalpy,
Assumed $d^* = 0.200 \pm 0.004$ in.

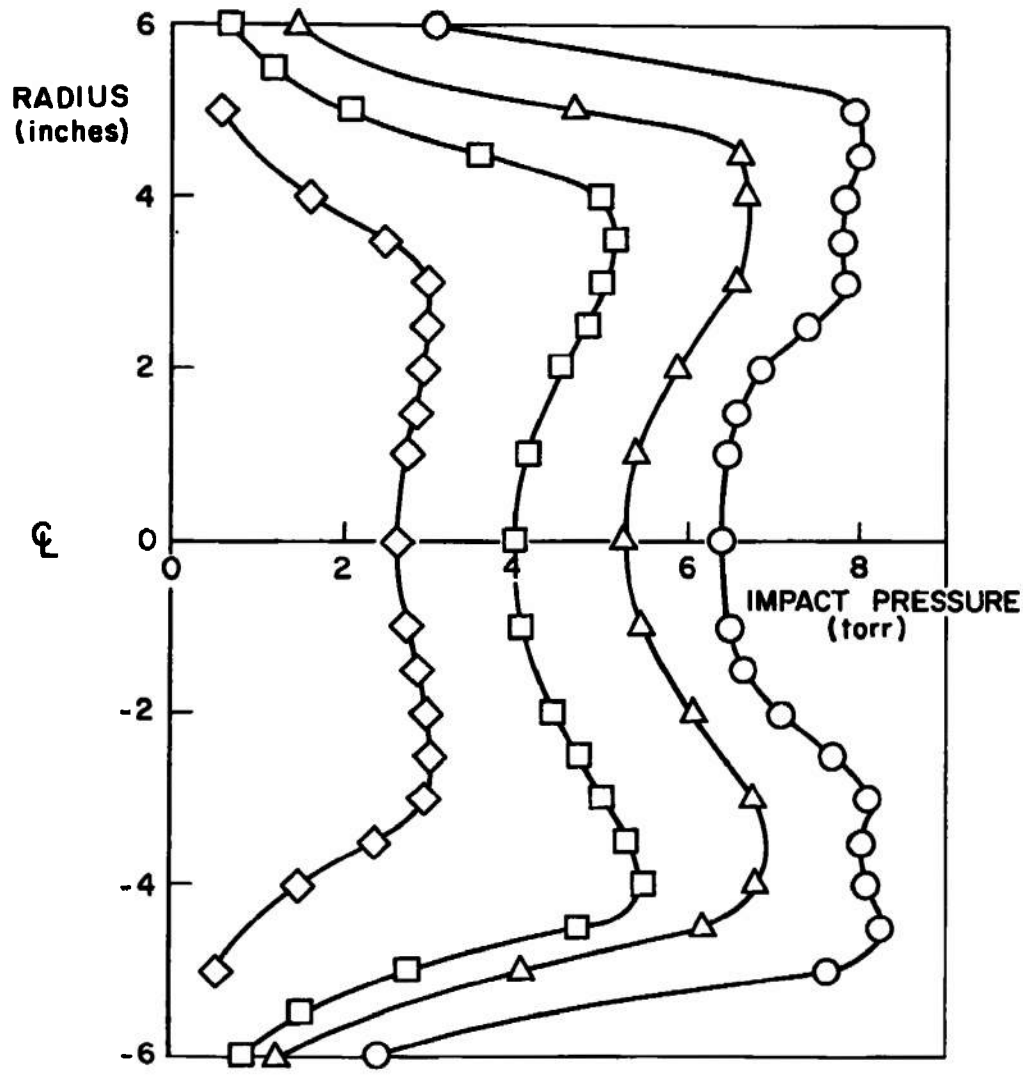


Fig. 9 Impact Pressure Profiles across the Flow at the Nozzle Exit

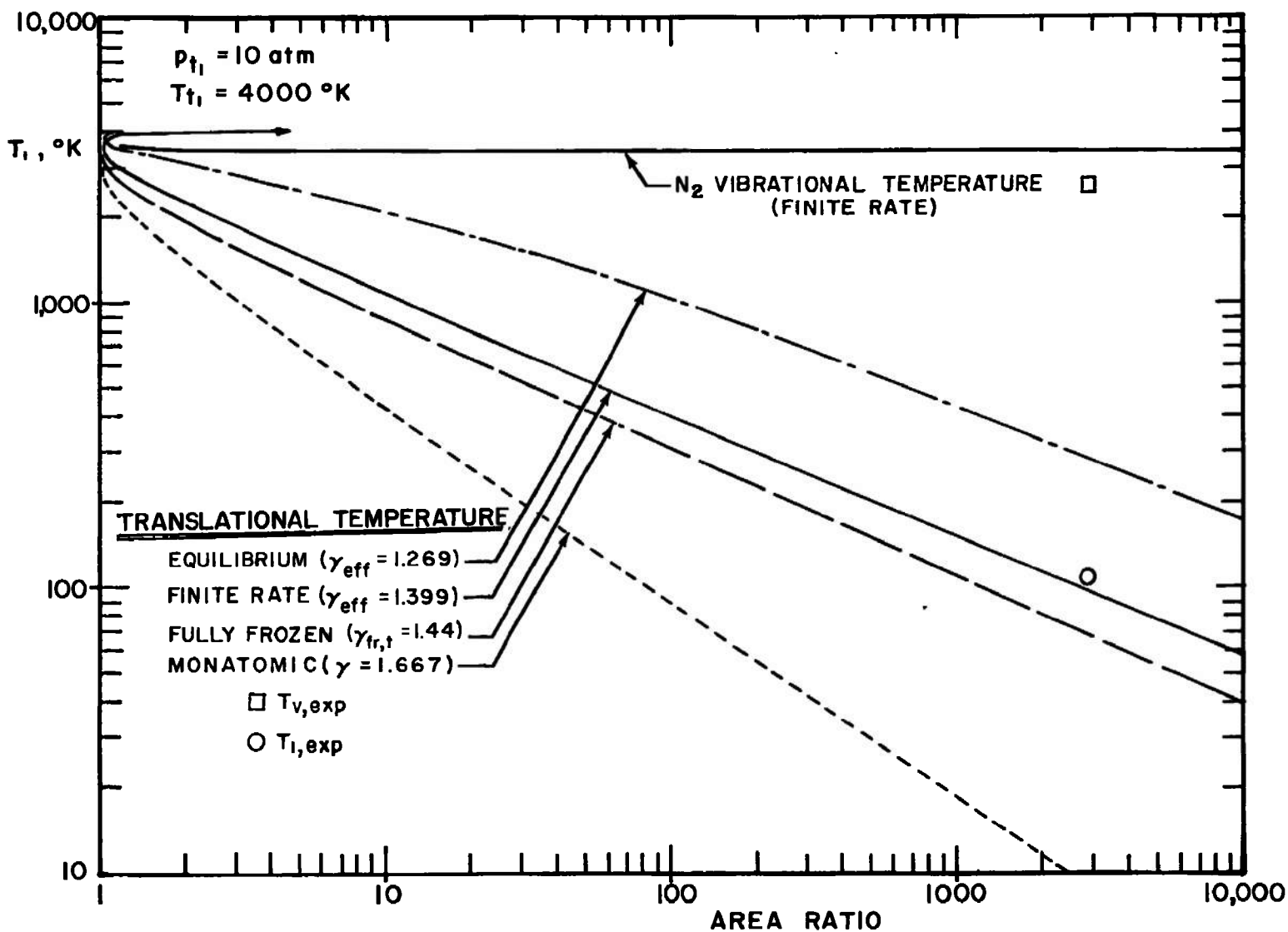


Fig. 10 Static Temperature versus Area Ratio for Various Types of Expansion, $p_{t1} = 10 \text{ atm}$, $T_{t1} = 4000^\circ\text{K}$

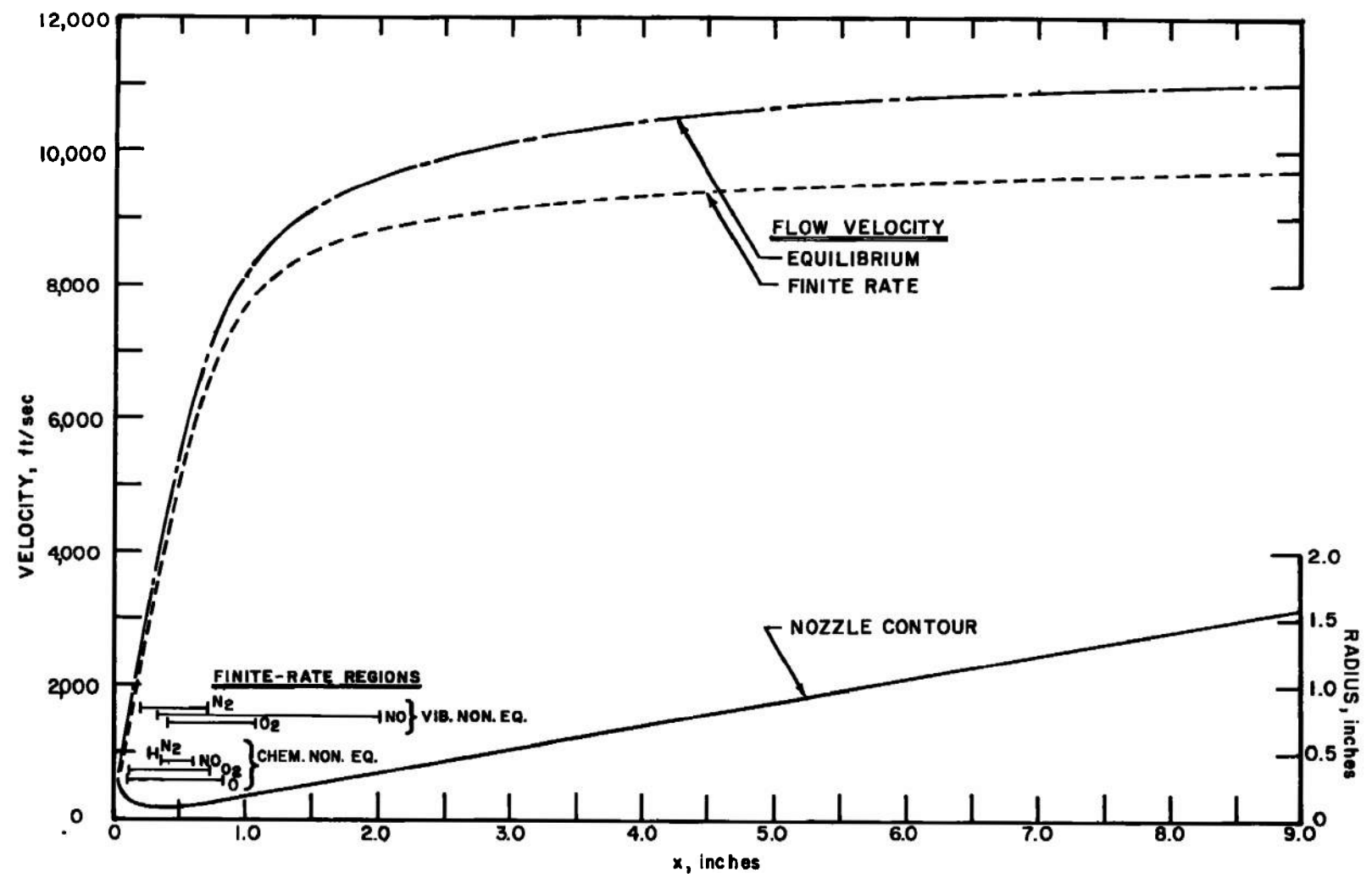


Fig. 11 Finite-Rate Flow Regions and Velocity in Nozzle, $p_{t1} = 10 \text{ atm}$, $T_{t1} = 4000^\circ\text{K}$

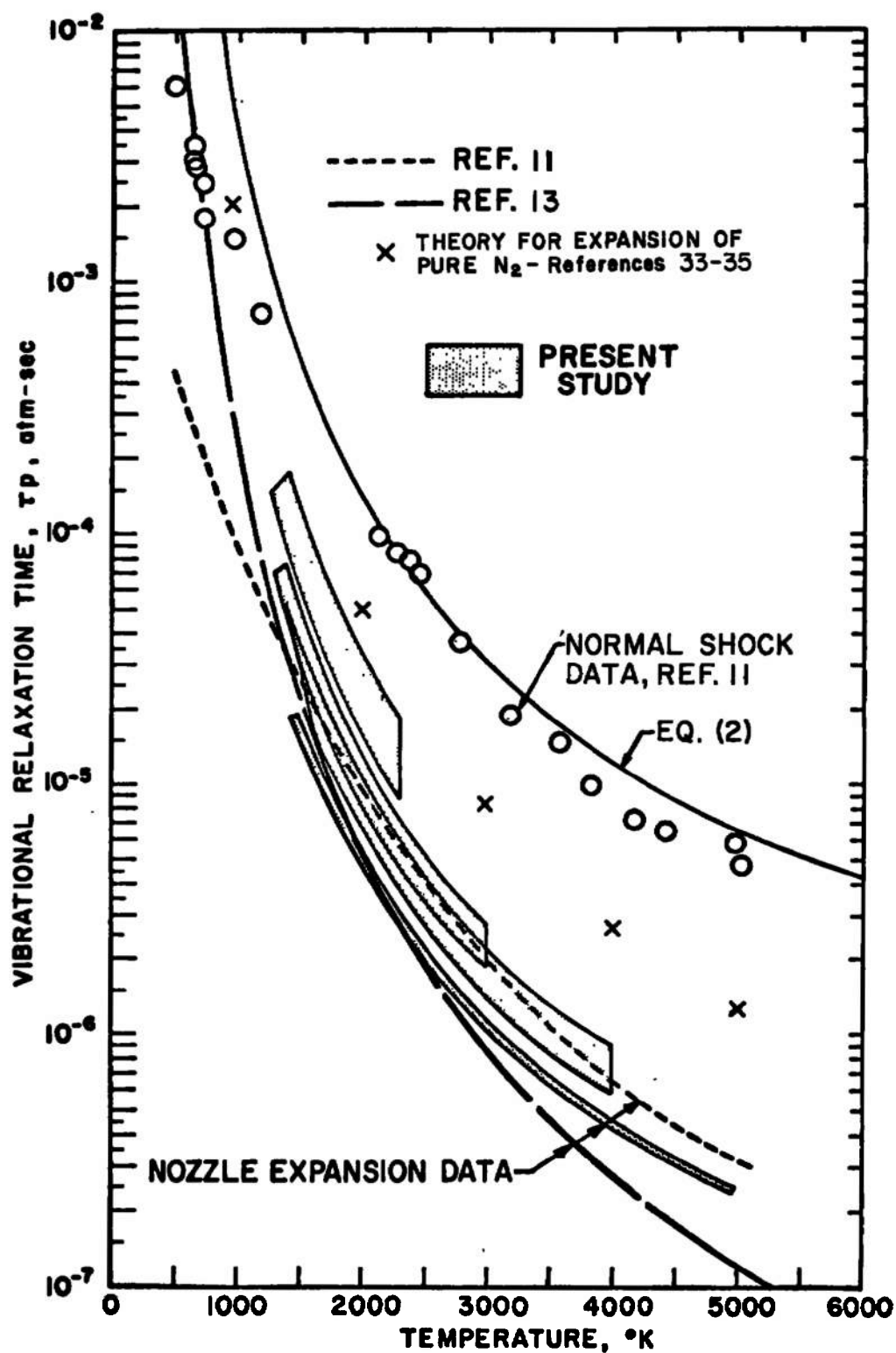
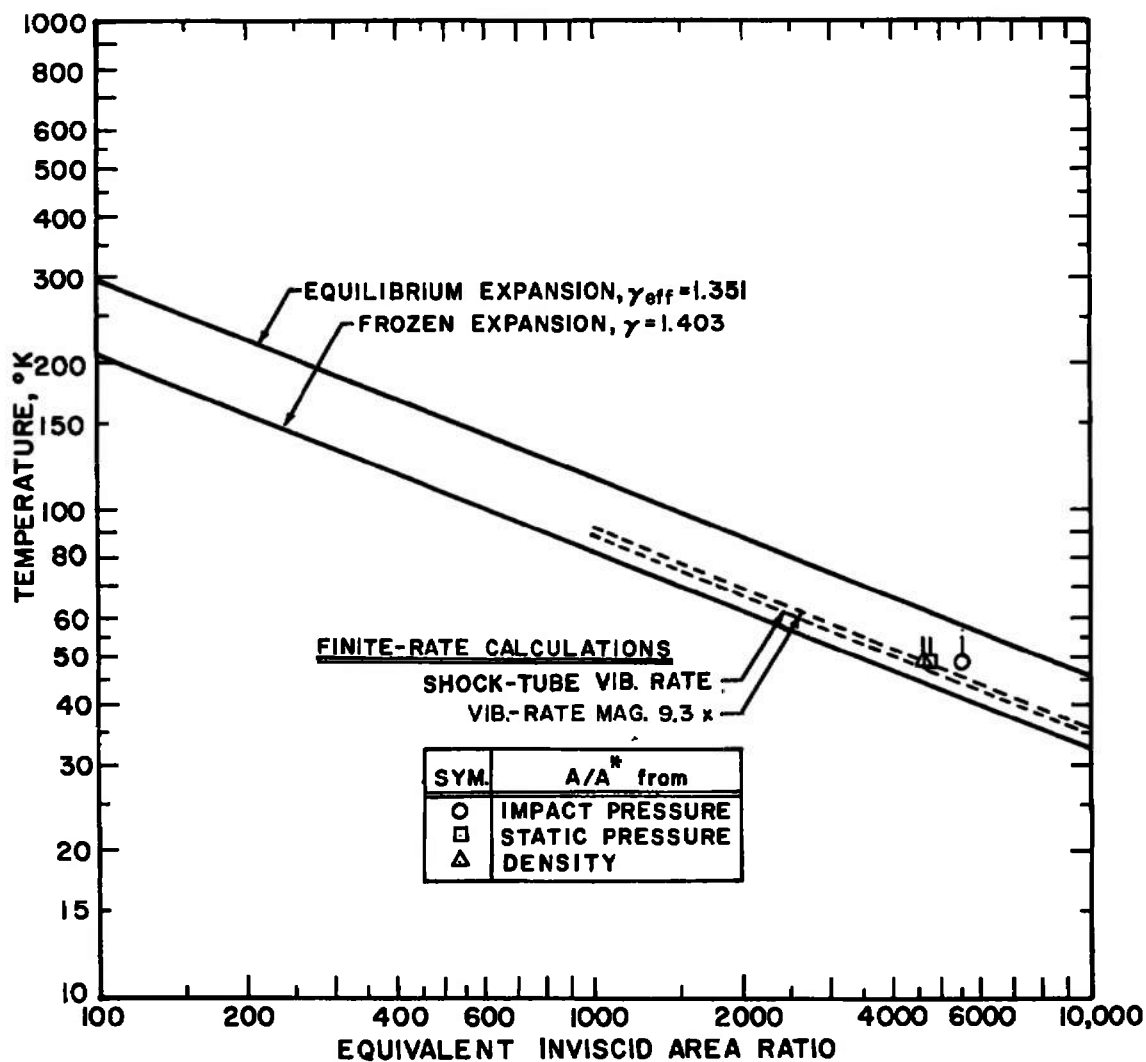
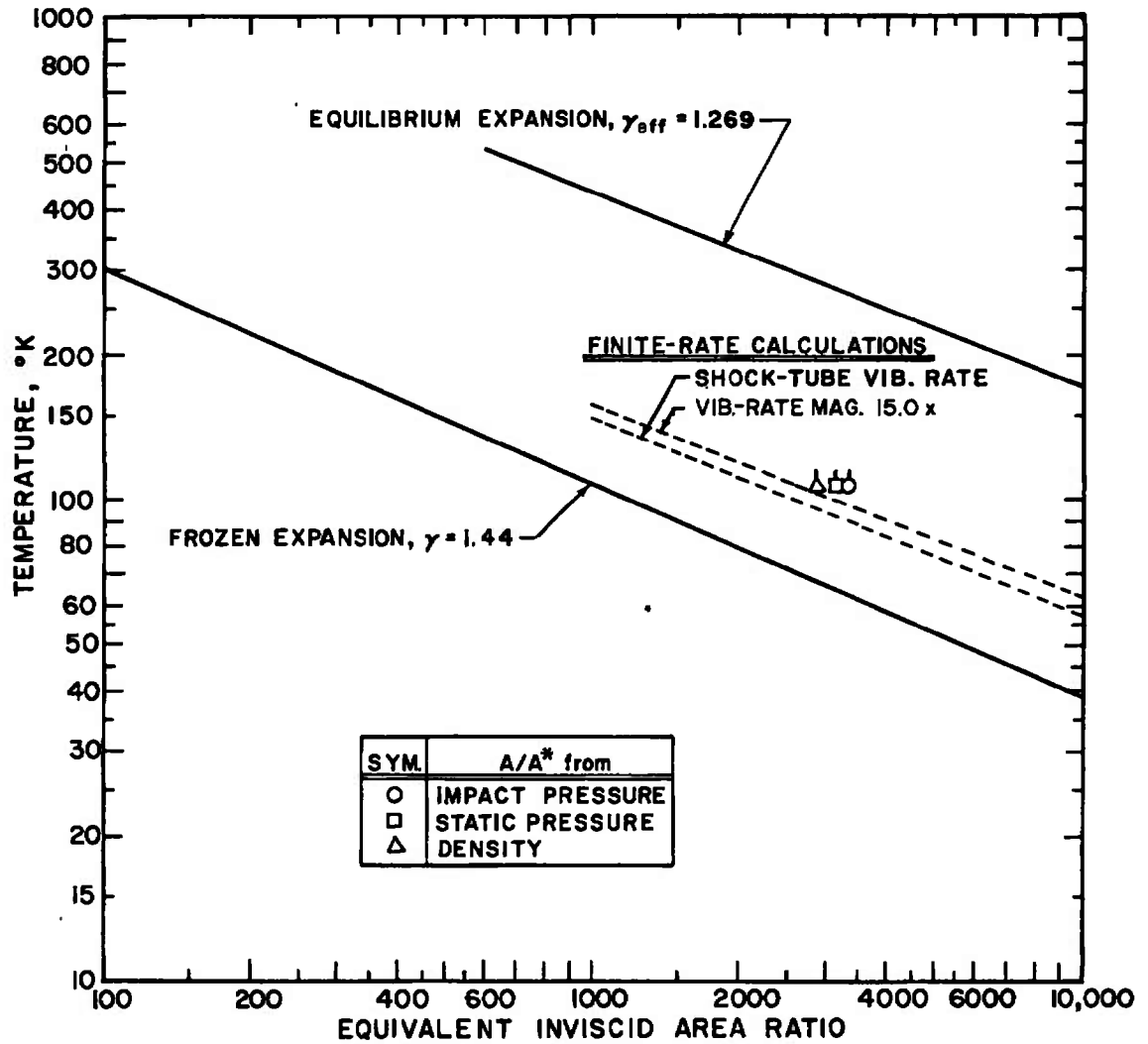


Fig. 12 Nitrogen Vibrational Relaxation Time Factor versus Temperature



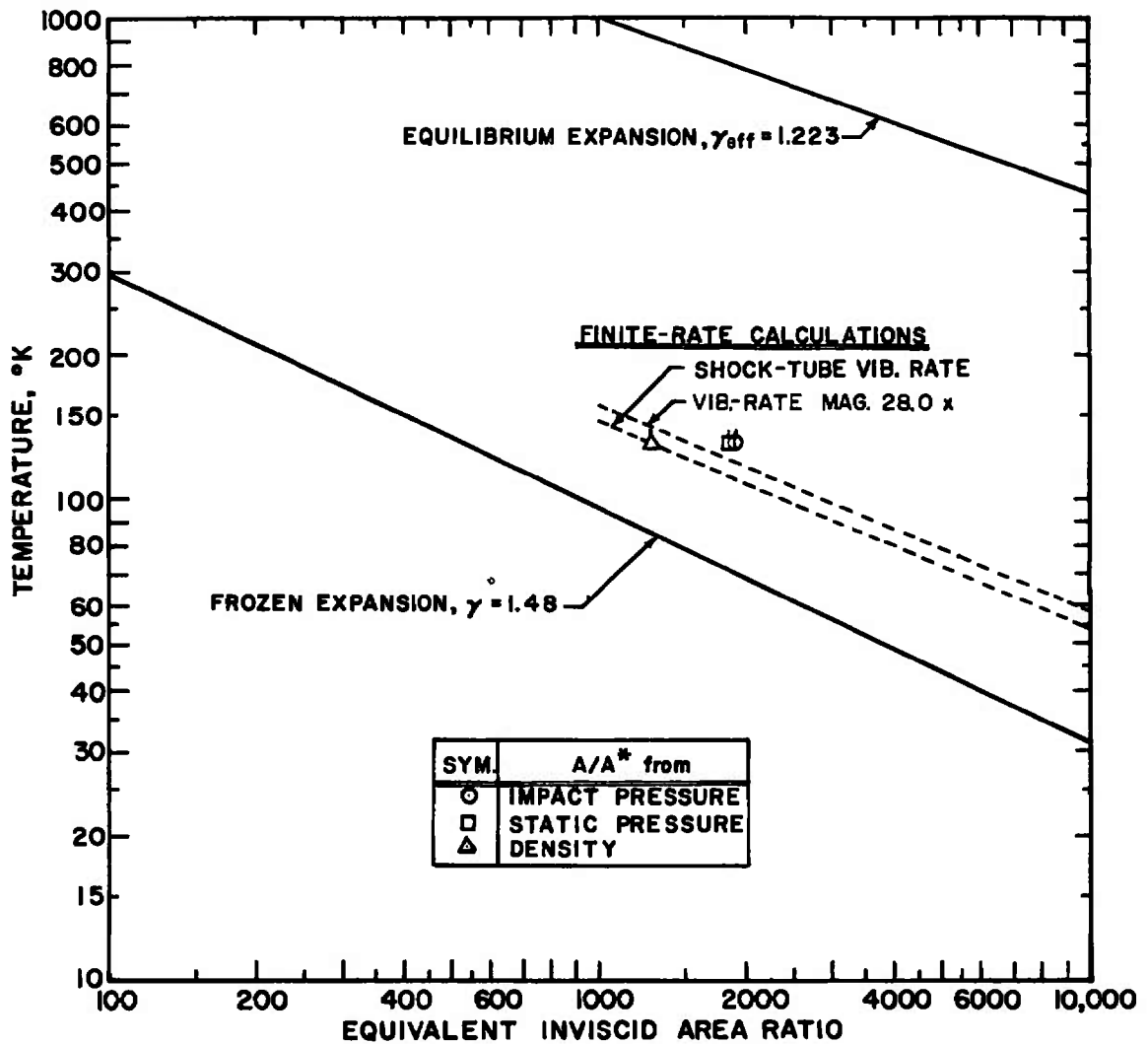
$$a. p_{t_1} = 20 \text{ atm}, T_{t_1} = 2300^\circ\text{K}$$

Fig. 13 Experimental and Theoretical Static Temperature versus Area Ratio



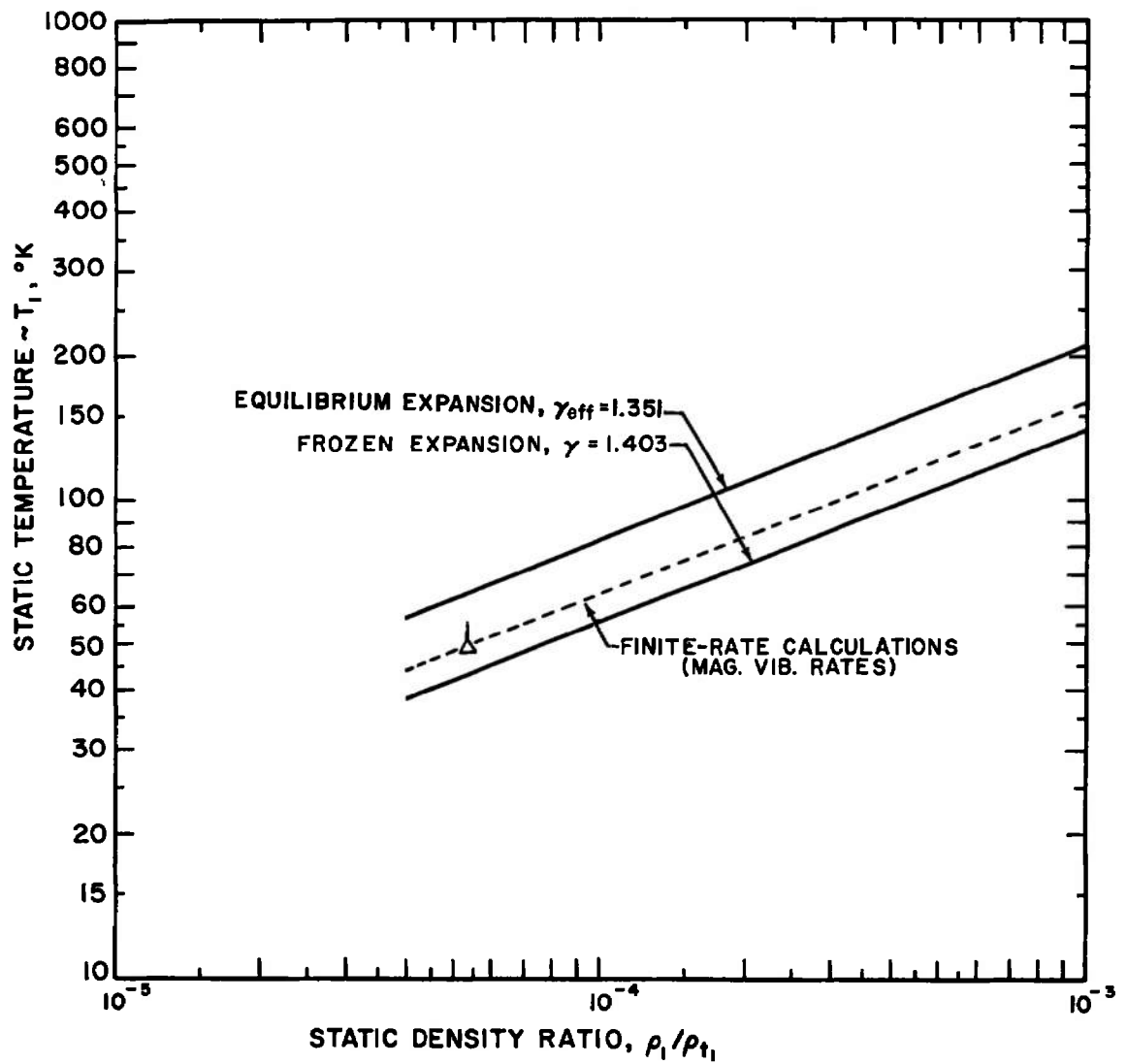
b. $p_{t_1} = 10 \text{ atm}$, $T_{t_1} = 4000^\circ\text{K}$

Fig. 13 Continued



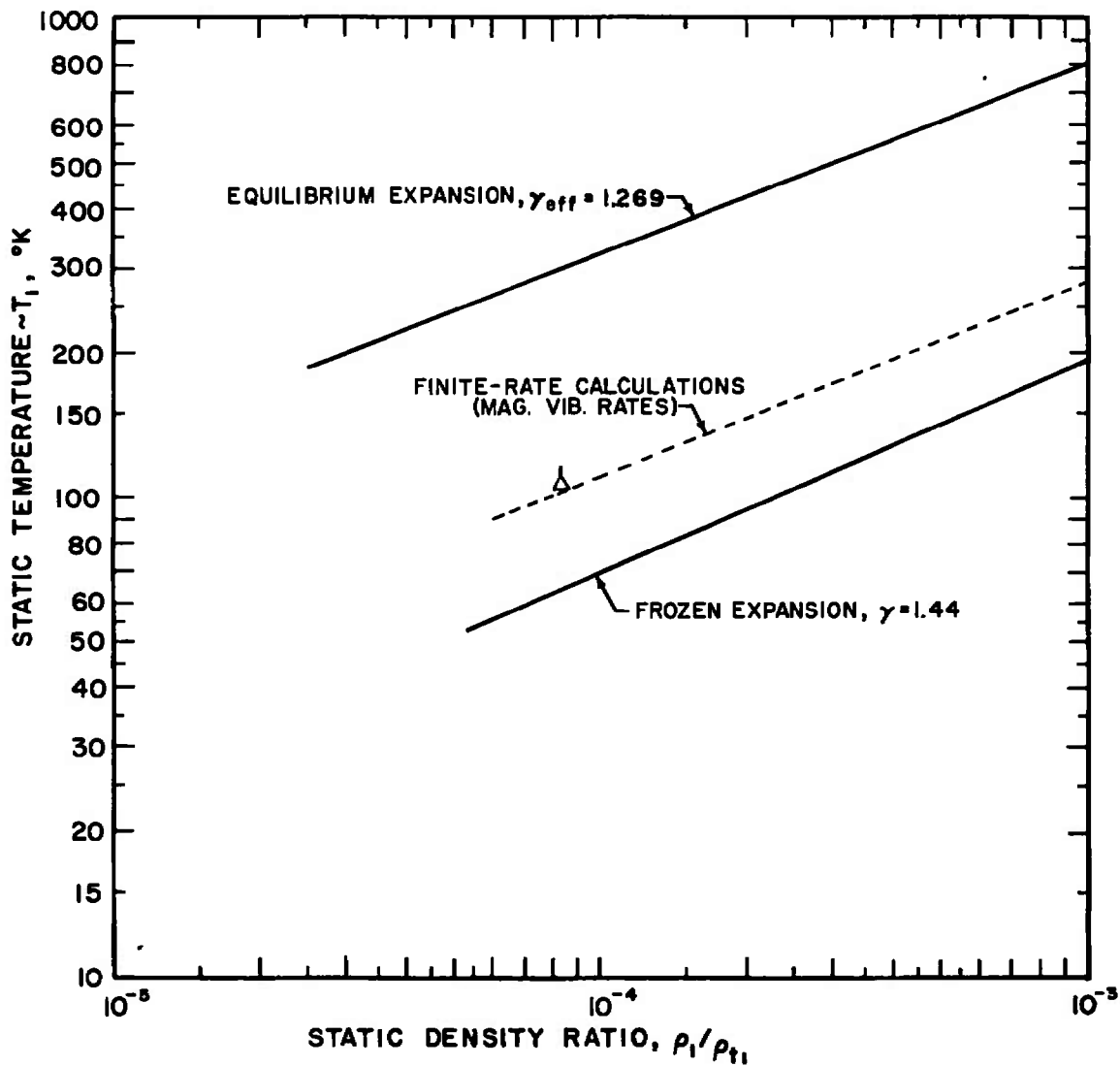
c. $p_{t1} = 5 \text{ atm}$, $T_{t1} = 5000^\circ\text{K}$

Fig. 13 Concluded



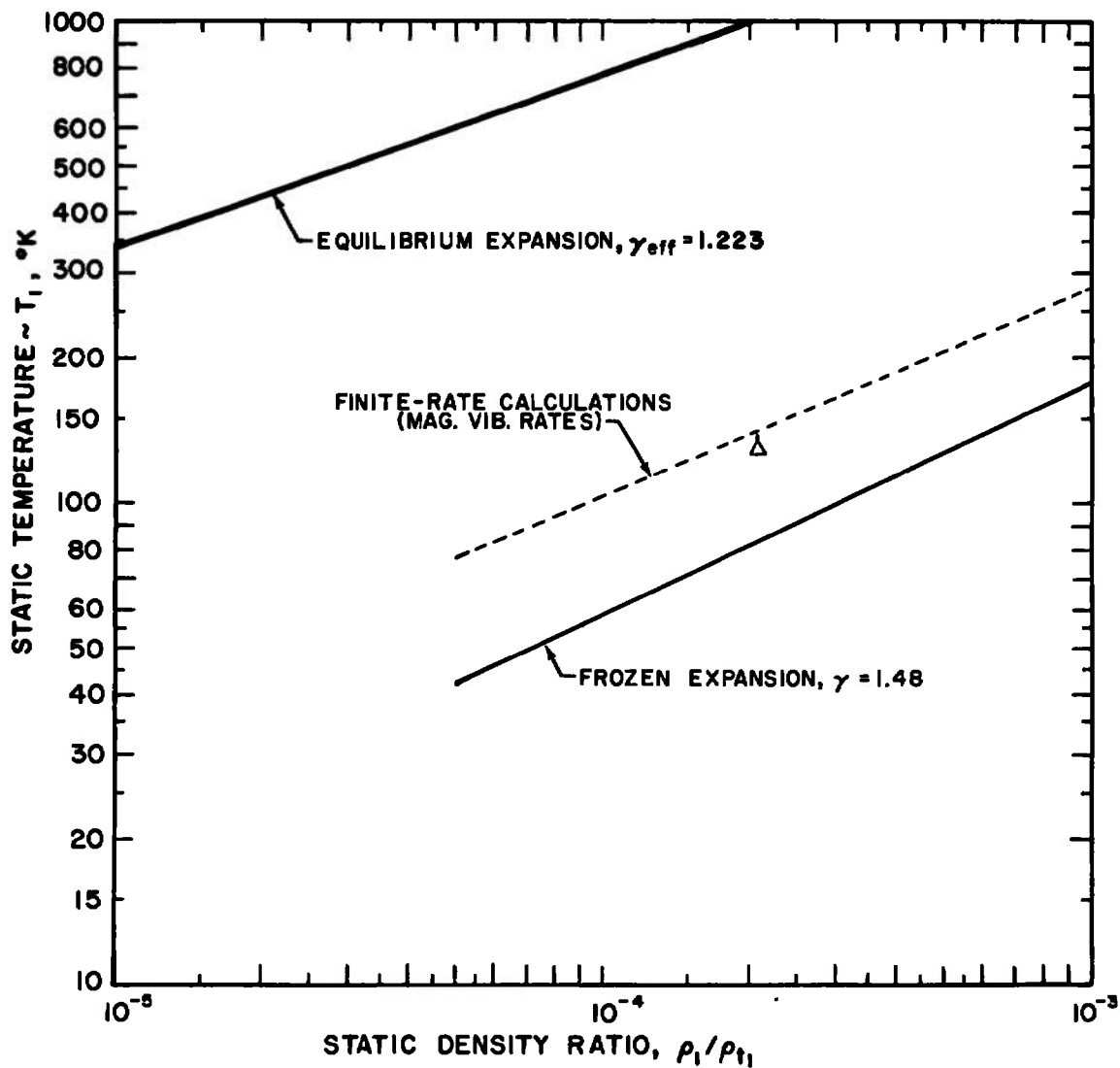
a. $p_{t_1} = 20 \text{ atm}$, $T_{t_1} = 2300^\circ\text{K}$

Fig. 14 Experimental and Theoretical Static Temperature versus Static Density



b. $p_{t_1} = 10 \text{ atm}$, $T_{t_1} = 4000^\circ\text{K}$

Fig. 14 Continued



c. $p_{t1} = 5 \text{ atm}$, $T_{t1} = 5000^\circ\text{K}$

Fig. 14 Concluded

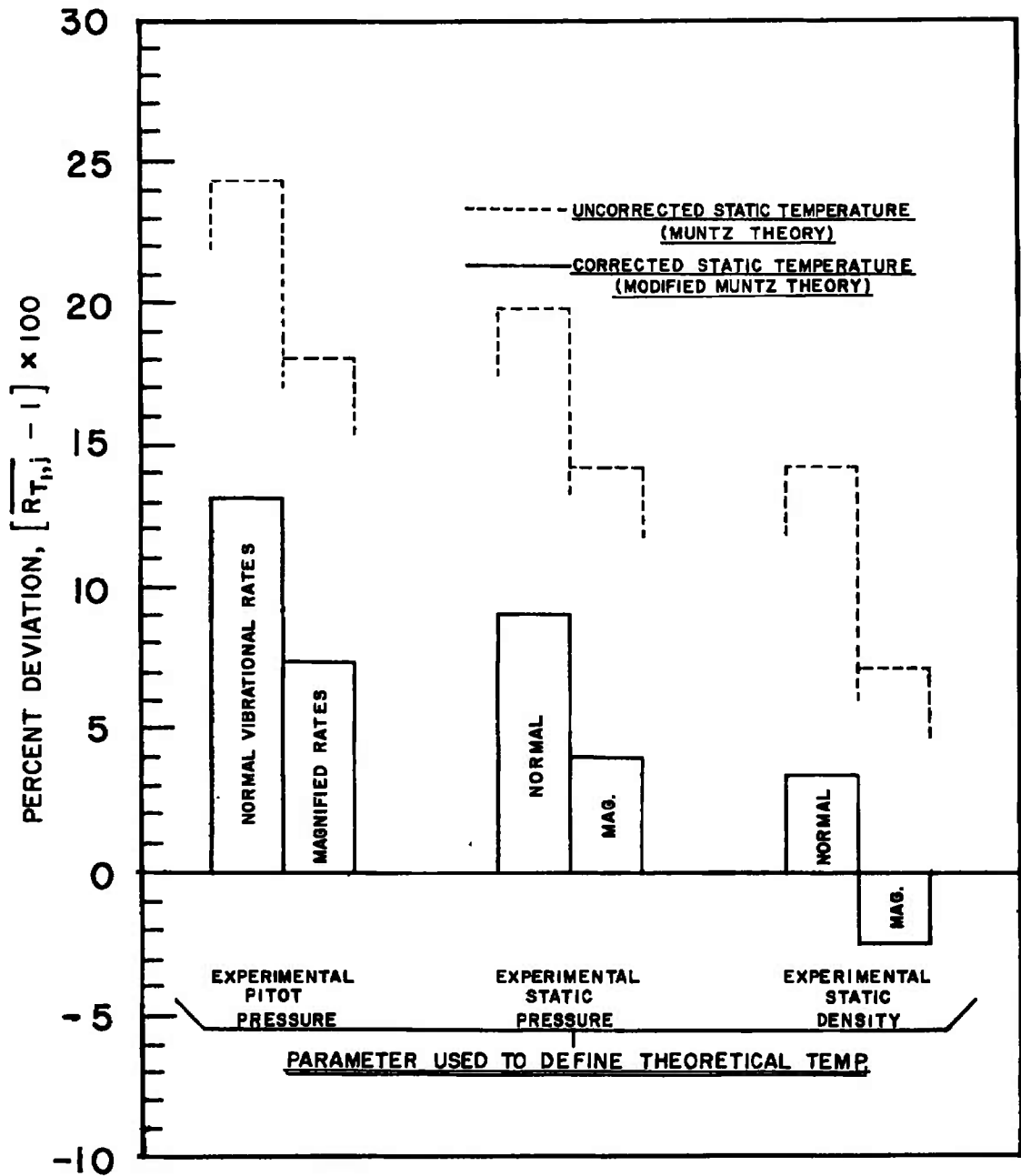
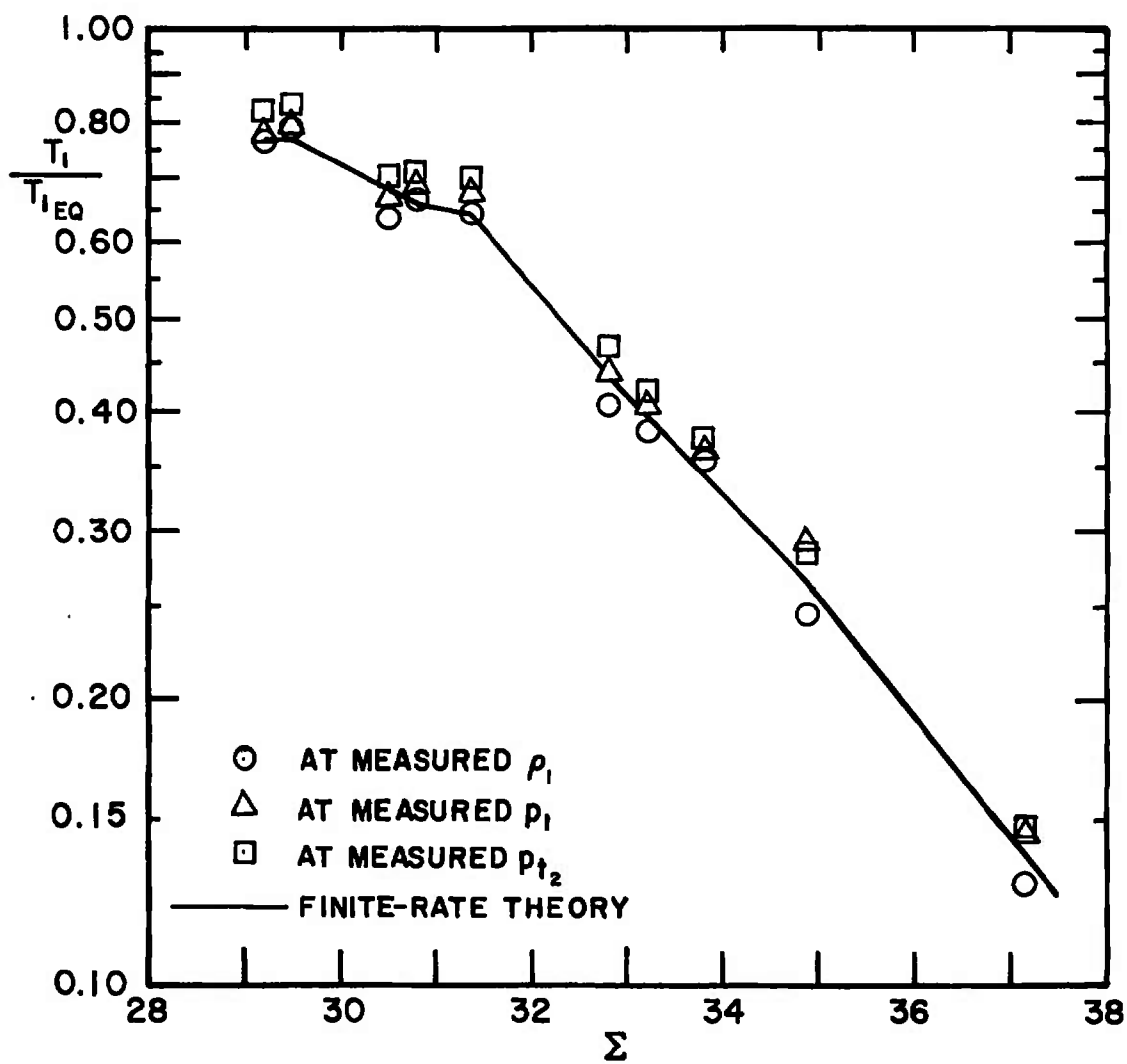


Fig. 15 Average Deviation of Measured Static Temperature from Finite-Rate Theory for Ten Reservoir Conditions, $p_{t,1} = 5$ to 20 atm, $T_{t,1} = 2300$ to 5000°K



a. T_1/T_{1EQ} versus Σ

Fig. 16 General Correlation of Finite-Rate Effect on Static Temperature and Static Pressure

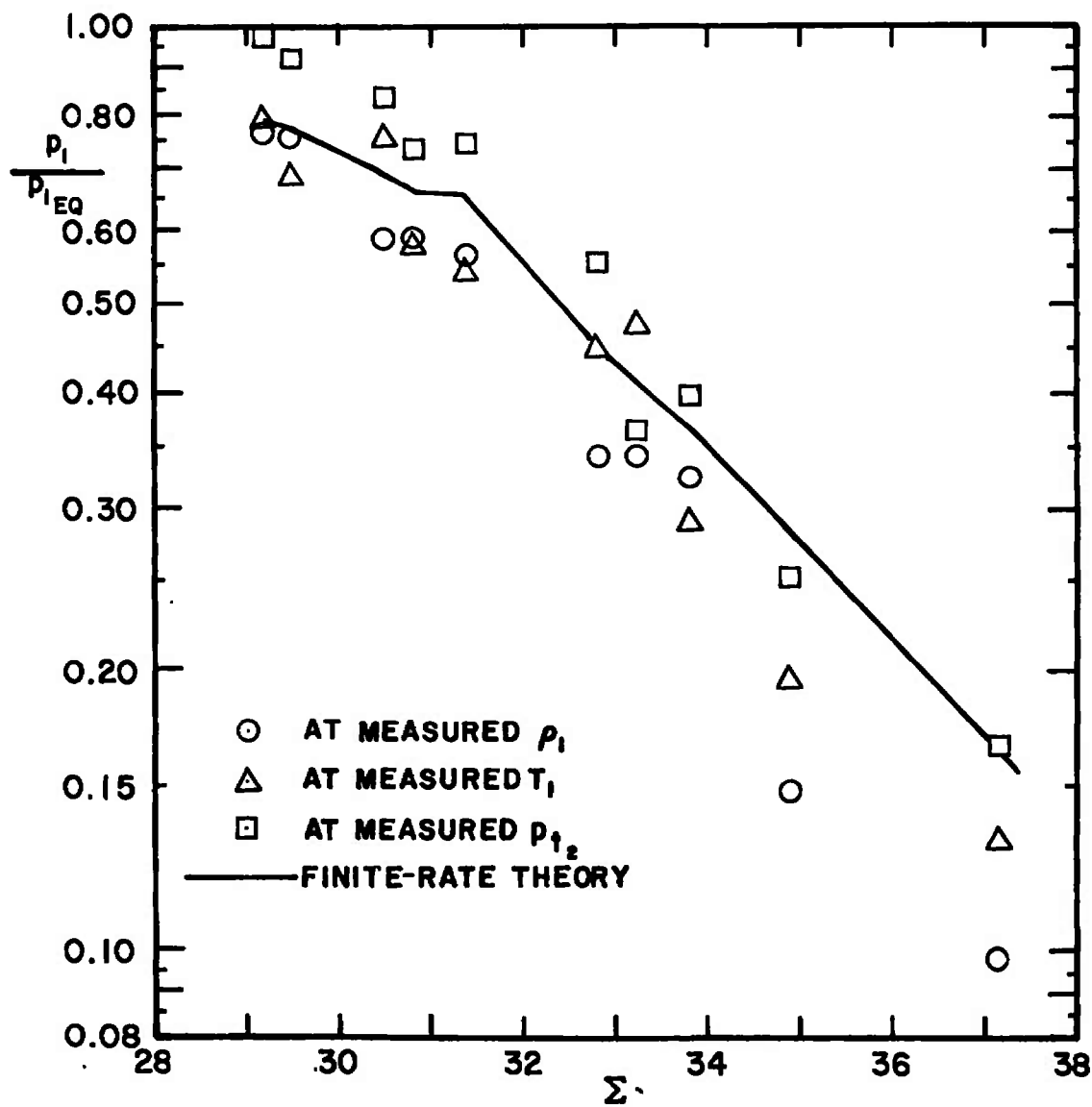
b. p_1/p_{1EQ} versus Σ

Fig. 16 Concluded

TABLE I
SUMMARY OF RESERVOIR CONDITIONS AND MEASUREMENTS AT NOZZLE EXIT

Reservoir Conditions							Vibrational Temperature			Static (Rotational) Temperature	
Point	Pt ₁ , atm	T _{t1} , °K	H _{t1} , Btu/lb _m	Z	$\gamma_{fr,t}$	Σ	Experimental, °K	Theoretical (Normal Rates) °K	Magnification Factor Required	Measured, °K	Corrected, °K
1	15	2300	1154	1.0003	1.403	29.47	1937	2132	4.4x	58.3	51.4
2	20	2300	1154	1.0002	1.403	29.18	1777	2099	9.3x	55.8	48.9
3	10	3000	1635	1.008	1.407	31.34	2228	2701	11.0x	83.2	75.3
4	15	3000	1625	1.006	1.406	30.79	2136	2630	11.3x	81.8	73.9
5	20	3000	1619	1.005	1.4055	30.48	1983	2575	17.0x	76.1	68.4
6	5	4000	2911	1.096	1.449	34.87	2682	3587	22.5x	123.3	114.5
7	10	4000	2755	1.075	1.440	33.80	2592	3433	15.3x	115.2	106.5
8	15	4000	2676	1.064	1.434	33.21	2508	3331	14.0x	112.7	104.0
9	20	4000	2625	1.057	1.431	32.80	2373	3257	16.0x	110.8	102.1
10	5	5000	4157	1.182	1.484	37.14	2933	4267	28.0x	139.2	130.3

Static Density			Static Pressure			Pitot Pressure	
Point	$(\rho_t/\rho_{t1})_{exp}$	Inferred A/A*	$(p_1/p_{t1})_{exp}$	$(p_1/p_{t1})_{corr}$	Inferred A/A*	$(p_{t2}/p_{t1})_{exp}$	Inferred A/A*
1	5.75×10^{-5}	4350	1.73×10^{-6}	1.23×10^{-6}	4410	3.31×10^{-4}	5000
2	5.35×10^{-5}	4610	1.61×10^{-6}	1.12×10^{-6}	4760	3.02×10^{-4}	5510
3	7.23×10^{-5}	3410	2.1×10^{-6}	1.55×10^{-6}	3810	4.0×10^{-4}	4180
4	6.6×10^{-5}	3710	1.96×10^{-6}	1.43×10^{-6}	4060	3.81×10^{-4}	4340
5	6.2×10^{-5}	3910	1.79×10^{-6}	1.29×10^{-6}	4410	3.36×10^{-4}	5040
6	17.5×10^{-5}	1410	2.73×10^{-6}	2.85×10^{-6}	2210	8.03×10^{-4}	2040
7	8.3×10^{-5}	2870	2.34×10^{-6}	1.88×10^{-6}	3150	5.02×10^{-4}	3330
8	7.5×10^{-5}	3150	2.13×10^{-6}	1.62×10^{-6}	3610	4.23×10^{-4}	3980
9	7.42×10^{-5}	3120	2.03×10^{-6}	1.55×10^{-6}	3810	3.85×10^{-4}	4410
10	20.7×10^{-5}	1280	2.85×10^{-6}	3.47×10^{-6}	1860	9.36×10^{-4}	1905

TABLE II
REACTIONS INCLUDED IN FINITE-RATE FLOW MODEL

Reaction	C ₁	C ₂	C ₃	n
$O_2 + O_2 \rightleftharpoons 2O + O_2$	8.0×10^{13}	-3/2	0	2
$O_2 + O \rightleftharpoons 2O + O$	2.3×10^{14}	-3/2	0	2
$O_2 + N_2 \rightleftharpoons 2O + N_2$	6.2×10^9	-1/2	0	2
$O_2 + N \rightleftharpoons 2O + N$	3.0×10^9	-1/2	0	2
$O_2 + NO \rightleftharpoons 2O + NO$	3.0×10^9	-1/2	0	2
$N_2 + O_2 \rightleftharpoons 2N + O_2$	1.1×10^{10}	-1/2	0	2
$N_2 + O \rightleftharpoons 2N + O$	1.1×10^{10}	-1/2	0	2
$N_2 + N_2 \rightleftharpoons 2N + N_2$	2.8×10^{10}	-1/2	0	2
$N_2 + N \rightleftharpoons 2N + N$	2.4×10^{15}	-3/2	0	2
$N_2 + NO \rightleftharpoons 2N + NO$	1.1×10^{10}	-1/2	0	2
$NO + O_2 \rightleftharpoons N + O + O_2$	1.0×10^{14}	-3/2	0	2
$NO + O \rightleftharpoons N + O + O$	1.0×10^{14}	-3/2	0	2
$NO + N_2 \rightleftharpoons N + O + N_2$	1.0×10^{14}	-3/2	0	2
$NO + N \rightleftharpoons N + O + N$	1.0×10^{14}	-3/2	0	2
$NO + NO \rightleftharpoons N + O + NO$	2.0×10^{15}	-3/2	0	2
$O + N_2 \rightleftharpoons NO + N$	1.6×10^{10}	0	0	1
$NO + O \rightleftharpoons N + O_2$	1.3×10^7	1	-3560	1
$N_2 + O_2 \rightleftharpoons 2NO$	2.4×10^{20}	-5/2	-43,000	1

Equilibrium Reverse Reaction Rate Constant

$$(k_r)_{EQ} = \left[C_1 T^{C_2} \exp \left(\frac{C_3}{T} \right) \right] \left(\frac{\text{meter}^3}{\text{kg-mole}} \right)^n / \text{sec}$$

APPENDIX III

TEMPERATURE MEASUREMENTS BY THE ELECTRON-BEAM TECHNIQUE

If a low density gas is bombarded by a high energy (10- to 30-kv) beam of electrons, the resulting emission can be analyzed to infer the gas temperature. To date, the only gases studied by this technique have been N_2 or N_2 -rich mixtures, using the analysis procedure developed by Muntz (Ref. 15). The nitrogen ion (N_2^+) first negative emission system, roughly centered at 3900 Å, is very intense in the emission of air excited by an electron beam. Muntz proposed a simple excitation/emission model for this emission system in which the excited N_2^+ ions forming the upper state of the emission were produced by direct excitation of ground state neutral N_2 molecules in collision with the high-speed electrons of the beam. The excited ions were assumed to undergo spontaneous emission to the ionic ground state to produce the first negative system, and both excitation and emission were assumed to obey optical selection rules. The three molecular states involved have the following designations:

N_2 ground state ($N_2X^1\Sigma$), designated by a subscript g

N_2^+ excited state ($N_2^+B^2\Sigma$), designated by a single superscript

N_2^+ ground state ($N_2^+X^2\Sigma$), designated by a double superscript

ROTATIONAL TEMPERATURE

In most practical cases, the translational temperature of molecular motion is in equilibrium with the temperature characterizing the distribution of rotational energy states. The rotational temperature can be inferred from the electron-beam emission by analysis of the distribution of intensity of individual rotational lines within a single vibrational band. Based on the model described above, Muntz derived an expression for the intensity of a single rotational line:

$$I_{K', K'', v', v''} = \text{constant} \times N_0 \times f(v', v'', T_R, T_v) \times \bar{\nu}^{K', K'', v', v''} \times G(K', \theta_{rot}, T_R) \times K' \exp \left[-\frac{\theta_{rot}}{T_R} K'(K' + 1) \right] \quad (\text{III-1})$$

where $I_{K', K'', v', v''}$ is the intensity of emission resulting from a rotational state transition from K' to K'' levels, within a vibrational state transition from v' to v'' level. Since the analysis is confined to a specific vibrational band (usually 0, 0 band), the v' and v'' subscripts may be dropped. Since optical transition rules are adopted, $\Delta K = \pm 1$ in

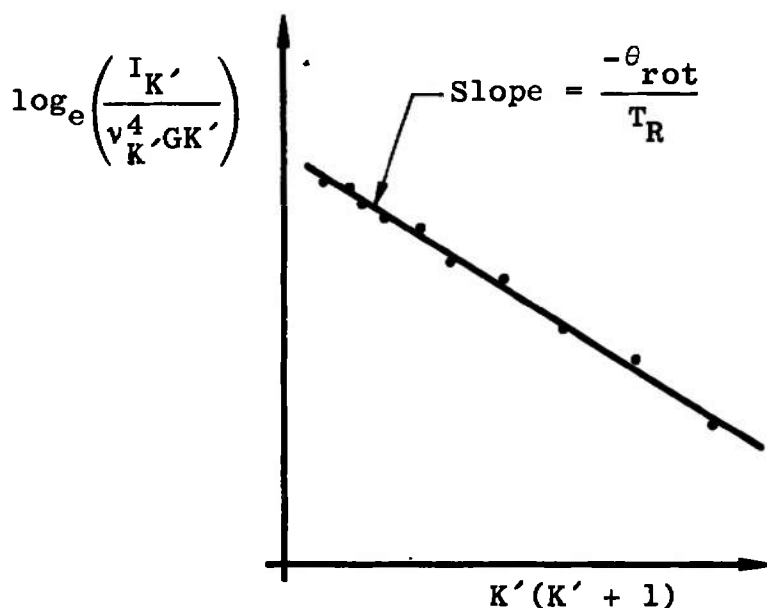
the transition, and Eq. III-1 has already been specialized to the case where $K'' = K' - 1$, the so-called R-Branch of the rotational transition. The product of K' and the exponential function in Eq. (III-1) is almost identical to the rotational state distribution of the unexcited N_2 molecules, but in the formation of the intensity distribution it is modified by the function,

$$G(K', \theta_{\text{rot}}, T_R) = \frac{K' - 1}{2K' + 1} \exp \left[\frac{-\theta_{\text{rot}}}{T_R} 2(K' + 1) \right] + \frac{K'}{2K' + 1} \exp \left[\frac{\theta_{\text{rot}}}{T_R} 2K' \right] \quad (\text{III-2})$$

The determination of T_R from measured $I_{K'}$ in a band involves the rearrangement of Eq. (III-1) and the taking of a natural logarithm:

$$\log_e \left[\frac{I_{K'}}{v_K^4 G K'} \right] = - \left(\frac{\theta_{\text{rot}}}{T_R} \right) K'(K' + 1) + \text{constant} \quad (\text{III-3})$$

Clearly, there is a linear relation between the logarithm on the left and the quantity $K'(K' + 1)$ so that a plot of the logarithm versus $K'(K' + 1)$ will be a straight line (see below) with a slope equal to $-\theta_{\text{rot}}/T_R$, where θ_{rot} for ground state N_2 at $v_g = 0$ is 2.89°K . The "constant" on the right side of Eq. (III-3) is a function of many variables: electron-beam characteristics, N_0 , the specific vibrational transition, T_v and T_R . This constant determines the intercept on the ordinate but has no effect on the slope of the line. The function, G , is weakly dependent on T_R , necessitating an iteration to obtain a consistent value of T_R . There is, for this particular emission system, a 2:1 intensity ratio for alternating lines, resulting from nuclear statistics. This phenomenon is usually compensated for by multiplying the half-strength lines by a factor of 2.0.



This procedure, while simple and straightforward in theory, has proved to be somewhat less than simple to apply in practice. Muntz applied the technique to measure static temperature in both arc-heated and cold low density flows, and it was rapidly adopted by other laboratories (Refs. 9, 10, 12, 16, and 17). Several anomalies were discovered when the technique was extended to temperature regimes not covered in Muntz's original experiment. First of all, at temperatures below 150°K the logarithmic intensity plots were found to exhibit a pronounced upward curvature which increased as absolute temperature was decreased. Second, even when straight lines were drawn tangent to these curves, the indicated T_R was invariably in excess of the gas temperature obtained by gas dynamics calculations, and the excess also increased as temperature decreased. Since these effects were first observed in low temperature free jets and nozzle flows (Ref. 16), the possibility of rotational nonequilibrium in the flow expansions was suggested. This possibility was eliminated, however, by an extensive experiment conducted in a static test chamber at temperatures down to 80°K (Ref. 20). The same results were found as for a flowing gas, except that an additional dependence of the divergence of T_R and gas temperature on static density was found. A number of possible explanations of these effects has been investigated, including a complete reformulation of the excitation model (Ref. 38), but their source still remains uncertain.

At very low temperatures (10 to 20°K) the divergence of T_R and gas temperature is as large as 40 percent, but at the temperatures normally encountered in the 18-in. low density wind tunnel (100°K), it is only approximately 8 percent. The measured temperatures are easily corrected by use of an empirical correction curve, as suggested in Ref. 16. The density dependence of the divergence is rather small (5 percent in an order of magnitude), so that it is usually possible to use a single correction curve over the entire range of operation of a given facility. In the present study, the correction curve of Ref. 16 was used directly, except for minor changes made to it at temperatures around 80°K, based on static calibrations in our own facilities. The wind tunnel test results have shown that the correction is indeed required and that the empirical correction of Ref. 16 appears to be of the proper magnitude.

VIBRATIONAL TEMPERATURE

The temperature characterizing the distribution of vibrational states of the unexcited N_2 molecules is obtained by reference to the total intensity (sum of all rotational lines) of a specific vibrational band in the N_2^+ emission. Using Muntz's excitation/emission model, it can be

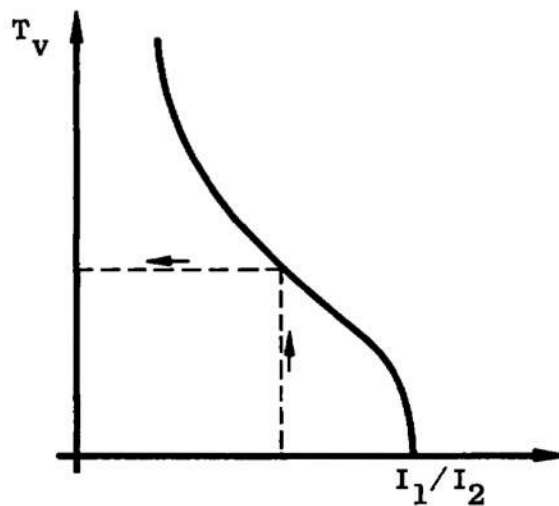
shown that the intensity of a complete vibrational band representing a transition between vibrational levels specified by the quantum numbers v' and v'' is:

$$I_{v', v''} = \text{constant} \times N_0 \times \frac{\bar{\nu}_v^4 P(v', v'')}{Q_v(T_v)} \frac{\sum_{v_g=0}^{\infty} \exp \left[-\frac{E_{v_g}}{kT_v} \right] P(v', v_g)}{\sum_{v''=0}^{\infty} \bar{\nu}_v^3 P(v', v'')} \quad (\text{III-4})$$

The ratio of intensity of two different bands is thus,

$$\frac{(I_{v', v''})_1}{(I_{v', v''})_2} = \left(\frac{\bar{\nu}_1}{\bar{\nu}_2} \right)^4 \frac{P_1(v', v'')}{P_2(v', v'')} \frac{\sum_{v_g=0}^{\infty} \exp \left[-\frac{E_{v_g}}{kT_v} \right] P_1(v', v_g)}{\sum_{v_g=0}^{\infty} \exp \left[-\frac{E_{v_g}}{kT_v} \right] P_2(v', v_g)} \times \left(\frac{\sum_{v''=0}^{\infty} \bar{\nu}_2^3 P_2(v', v'')}{\sum_{v''=0}^{\infty} \bar{\nu}_1^3 P_1(v', v'')} \right) \quad (\text{III-5})$$

For any two specific bands, $I_1/I_2 = f(T_v)$, a function which has the general shape shown below. For the present test, this curve was computed for the (0, 1)/(1, 2) band ratio and used to determine the T_v given in Table I.



Unfortunately, the transition probability factors for the vibrational transitions are not known with the same degree of accuracy as are the analogous factors for the rotational transitions, and there is considerable difference of opinion over the accuracy of T_v obtained by this procedure. Muntz originally quoted an accuracy of ± 5 percent, but later investigators have been less generous in their estimates, with values ranging from ± 10 to ± 20 percent (Refs. 9 and 10). Further, very little has been done to experimentally verify the measurements under the electron-beam conditions. A static calibration experiment is reported in Ref. 39 in which three points between 300 and 1100°K were obtained,

showing a divergence of from 1.5 to 16 percent from the theoretical curve. In Ref. 10, T_v obtained in wind tunnel flows using three different band ratios were found to have a scatter of ± 7 percent between the three ratios used. In the present study, a single comparison of T_v from two different band ratios showed a similar 7-percent difference. A recent study of the electron-beam temperature measurement technique, giving detailed derivations and results of validation experiments, is reported in Ref. 40.

APPENDIX IV DETERMINATION OF DENSITY BY ELECTRON BEAM

There are two types of electron-beam techniques which have sufficient accuracy and resolution to be used for wind tunnel diagnostics. The first of these utilizes the emission of the target gas as a measure of gas density. In Eqs. (III-1) and (III-4), it can be seen that both individual rotational lines and complete vibrational bands have intensities directly proportional to N_0 , the number density of neutral N_2 molecules. The various applications of this technique differ in the emission components used. Muntz used the intensity of a single rotational line in the (0, 0) band (Ref. 15). In Ref. 9 the total (0, 0) band strength was used, and in Ref. 10 the (0, 2) band was used. In Ref. 17, a number of bands were used simultaneously by means of a 100 Å half-width interference filter centered at the (0, 0) band. This technique is very easily calibrated by measurements in a static gas at precise values of pressure and temperature. If, however, the rotational and vibrational temperatures prevailing during the flow measurement are not the same as in the static calibration, correction factors are required which depend on these temperatures. This technique is also affected by any chemical changes in the gas which change the relative N_2 concentration.

The second type of density measurement, and the one used in the present study, is based on measurement of electrons elastically scattered at large angles out of the beam volume. A comprehensive description of the development of this technique is given in Ref. 19. The differential scattering cross section which an atomic nucleus presents to a high-speed electron, which penetrates the atom electron cloud and approaches the nucleus, is (Ref. 19)

$$d\sigma = \left(\frac{r_e}{2}\right)^2 Z^2 \frac{1 - \beta^2}{(\beta \sin \frac{\delta}{2})^4} d\Omega \quad (IV-1)$$

where the deflection is through an angle δ and into a solid angle of $d\Omega$. If an electron beam is directed into an extended region of target atoms of particle density n , there will result a field of scattered high-speed electrons surrounding the beam, with

$$\lambda = \frac{i n}{e} \left(\frac{r_e}{2}\right)^2 \frac{Z^2 (1 - \beta^2)}{(\beta \sin \frac{\delta}{2})^4} \Delta x \Delta\Omega \quad (IV-2)$$

where λ is the rate at which electrons are scattered from a small segment of the beam Δx into a solid angle $\Delta\Omega$ at an angle δ with respect to the incident beam. Rearranging this expression into convenient groups of variables,

$$\lambda = \left(\begin{array}{c} \text{electron count} \\ \text{rate at a} \\ \text{collimated} \\ \text{detector} \end{array} \right) = \left(\frac{r_e^2}{4e} \right) \cdot \left(\frac{i(1 - \beta^2)}{\beta^4} \right) \cdot \left(\frac{\Delta x \Delta \Omega}{(\sin \frac{\delta}{2})^4} \right) (nZ^2)$$

$$= \text{constant } f_1 \left(\begin{array}{c} \text{beam} \\ \text{characteristics} \end{array} \right) f_2 \left(\begin{array}{c} \text{detector-} \\ \text{collimator} \\ \text{characteristics} \end{array} \right) f_3 \left(\begin{array}{c} \text{target gas} \\ \text{characteristics} \end{array} \right) \quad (\text{IV-3})$$

The beam characteristics are determined by current and voltage, and the detector/collimator characteristics are mainly a matter of geometrical design. The target gas characteristic enters only as the atomic number of the nucleus and the particle density of the nuclei. In this model of the scattering process, based on deep penetration of the atom electron cloud, the distribution of nuclei through various chemical combinations does not affect the scattering process to first order. The mass density of a mixture can be expressed as

$$\rho = \frac{\sum n_i \Lambda_i}{N_a} \quad (\text{IV-4})$$

where the summation depends only on the total number of different types of atoms present in the mixture. Thus, a calibration of λ versus ρ made in low temperature air will still be valid at high temperature even though appreciable changes in detailed composition may have occurred.

UNCLASSIFIED

Security Classification

DOCUMENT CONTROL DATA - R & D

(Security classification of title, body of abstract and indexing annotation must be entered when the overall report is classified)

1. ORIGINATING ACTIVITY (Corporate author) Arnold Engineering Development Center ARO, Inc., Operating Contractor Arnold Air Force Station, Tennessee		2a. REPORT SECURITY CLASSIFICATION UNCLASSIFIED	
		2b. GROUP N/A	
3. REPORT TITLE NONEQUILIBRIUM NOZZLE EXPANSIONS OF PARTIALLY DISSOCIATED AIR: A COMPARISON OF THEORY AND ELECTRON-BEAM MEASUREMENTS			
4. DESCRIPTIVE NOTES (Type of report and inclusive dates) July 1967 to June 1968 - Final Report			
5. AUTHOR(S) (First name, middle initial, last name) W. N. MacDermott and J. C. Marshall, ARO, Inc.			
6. REPORT DATE July 1969		7a. TOTAL NO. OF PAGES 74	7b. NO. OF REFS 40
8a. CONTRACT OR GRANT NO. F40600-69-C-0001		9a. ORIGINATOR'S REPORT NUMBER(S) AEDC-TR-69-66	
b. PROJECT NO 4344			
c. Program Element 654021F		9b. OTHER REPORT NO(S) (Any other numbers that may be assigned this report) N/A	
d. Task 434402			
10. DISTRIBUTION STATEMENT This document has been approved for public release and sale; its distribution is unlimited.			
11. SUPPLEMENTARY NOTES Available in DDC.		12. SPONSORING MILITARY ACTIVITY Arnold Engineering Development Center Arnold AF Station, Tennessee 37389	
13. ABSTRACT A theoretical/experimental study was made of the rapid expansion of partially dissociated air in a high enthalpy wind tunnel. The theoretical model included the important nitrogen-oxygen reaction kinetics, as well as vibrational exchanges. Pressure measurements were supplemented by electron-beam measurements of static (translational) temperature, vibrational temperature, and static density. The primary result was general confirmation of finite-rate flow calculations. Secondly, rotational temperature determination by electron beam was found to require a small empirical correction, vibrational-relaxation rates from shock experiments were inapplicable in rapid flow expansion, and the static temperature/density combination yielded the optimum comparison with theory. The nonequilibrium data were correlated with an entropy parameter for reservoir pressures from 5 to 20 atm and temperature from 2300 to 5000°K. Verification of finite-rate theory at high density was inferred from data measured at large area ratios plus the simple nature of frozen flows downstream of the nozzle throat.			

DD FORM 1 NOV 65 1473

UNCLASSIFIED

Security Classification

14.	KEY WORDS	LINK A		LINK B		LINK C	
		ROLE	WT	ROLE	WT	ROLE	WT
	electron beams measurement air expansion nonequilibrium wind tunnels						